Spring 5-2010

Adaptive Cutting Force Control for Process Stability of Micro Ultrasonic Machining

Ala'a M. Al-okaily
UNL-IMSE, aokaily@gmail.com

ADAPTIVE CUTTING FORCE CONTROL FOR PROCESS STABILITY OF MICRO ULTRASONIC MACHINING

By

Ala'a M. Al-okaily

A THESIS

Presented to the Faculty of

The Graduate Collage at the University of Nebraska

In Partial Fulfillment of Requirements

For the Degree of Master of Science

Major: Manufacturing Systems Engineering

Under the Supervision of Professor Kamlakar P. Rajurkar

Lincoln, Nebraska

May, 2010

ADAPTIVE CUTTING FORCE CONTROL FOR PROCESS STABILITY OF MICRO ULTRASONIC MACHINING

Ala'a M. Al-okaily, M.S.

University of Nebraska, 2010

Advisor: Kamlakar P. Rajurkar

The growing demand for miniaturized products motivates the advancement in micromanufacturing processes research and development. Micro Ultrasonic Machining (Micro USM) is a downscaled version of a macro USM process that is developed to fabricate complex features in chemically inert, nonconductive, hard, brittle materials such as quartz, glass, and ceramics. These materials have many applications in various fields such as optics, electronics, MEMS, and biotechnology. The micro USM process stability is hard to accomplish, because it is highly influenced by the accuracy of the machining system and the variation of the process control parameters. The repeatability of micro USM machined features is greatly influenced by the cutting force variations. Therefore, designing a robust cutting force controller for the micro USM process is essential for stabilizing the material removal mechanism and improving machining characteristics.

A new micro USM machining system has been developed to enhance the cutting force control by improving the cutting force sampling and servo control frequencies. An Autoregressive Moving Average Model with Exogenous Input (ARMAX) is then used to develop a linear dynamic model for the micro USM cutting force based on experimental data. Proportional (P), Proportional-Integral (PI), and Model Reference Adaptive Control (MRAC) controllers are designed and implemented to stabilize the cutting force for the

micro USM process based on the ARMAX model. The process stability is analyzed to study the effects of these cutting force controllers on the micro USM cutting force stability, machining rate, and surface roughness of the machined features. The results show that the MRAC controller reduced both the cutting force variations (by 66% compared to the P controller) and the cutting force steady state error (< 1%). Moreover, the MRAC controller improves the repeatability of the micro USM machining characteristics.

ACKNOWLEDGEMENTS

I am thankful to my advisor Dr. Kamlakar P. Rajurkar for his continuous guidance, support, and for giving me the opportunity to work in The Centre for Nontraditional Manufacturing Research (CNMR).

I wish to thank my mentors at the CNMR, Dr. Murali Sundaram and Dr. Lin Gu for their help.

I also wish to thank my master thesis examination committee members, Dr. Fred Chobineh and Dr. John Boye for their time and suggestions.

I would like to thank all the IMSE department faculty members, staff, and co-researchers at The Centre for Nontraditional Manufacturing Research for providing me with a nice and friendly atmosphere that made my stay more comfortable.

I also wish to thank all my friends in Lincoln for their continuous support that gave me comfort.

I would like to thank all my family members especially my sisters and brothers for their care, trust, and support.

Finally, I dedicate this thesis to my parents for their trust and support that advanced my personal, academic, and professional life.

TABLE OF CONTENTS

LIST OF FIGURES

LIST OF TABLES

CHAPTER 1

INTRODUCTION

1.1 Micromanufacturing

Recently demand for miniaturized products has led to development and advancement in many micromanufacturing processes. For different workpiece materials, different manufacturing processes are required. The micromanufacturing processes, similar to the macro scale processes, can be classified as material addition processes, material removal processes, and material forming processes.

The machining processes are the most common manufacturing processes used to produce complex and high aspect ratio features for various workpiece material classes (e.g. metals, polymers, and ceramics). Along with other factors such as the process capability, machining productivity, surface quality, and dimensional accuracy, the workpiece material is a key parameter usually used to select the required machining process for generating a certain feature shape. In general, the conventional cutting processes (milling, turning, and drilling) are the best alternatives when the workpiece materials are relatively softer than the tool materials. Using the conventional machining processes, it is impossible or difficult to machine hard materials such as glass, silicon, quartz, ceramics, and titanium alloys. Sometimes it is essential to use these hard materials for certain applications where it is difficult to replace these materials with other alternatives. For example, ceramics are one of the most biocompatible materials widely used to make implant devices in the biotechnology field. Therefore, the nonconventional machining processes were proposed to machine these hard materials.

Almost all machining processes, conventional and nonconventional, were downscaled to meet the demand for machining micro features and parts. The Micro Ultrasonic Machining (Micro USM) process has recently been downscaled to fabricate complex and high quality micro features in hard and brittle materials. The micro USM process is also known as micro ultrasonic assisted lapping, micro ultrasonic impact grinding, and micro ultrasonic drilling.

1.2 Why Micro USM?

Figure 1.1 shows the machining process selection flow diagram for the most common machining processes based on the workpiece material properties. The advantages of using the micro USM process over the other micromachining processes are:

1. Complex shape features can be machined using any hard material regardless of the electrical, chemical, or thermal properties of the workpiece materials.
2. Since the USM process is a non-electrical and non-thermal machining process, high surface quality micro features can be achieved without surface cracks or thermal damages (e.g. heat affected zone). Moreover, the surface roughness of the machined features is low (down to ~ 0.2 μm) compared to the other micromachining processes.
3. The applied mechanical stress on the workpiece surface during machining is low compared to the other mechanical machining processes. Therefore, the produced parts experience fewer residual stresses that lead to more reliable parts.
4. The micro USM is an environmentally friendly process.

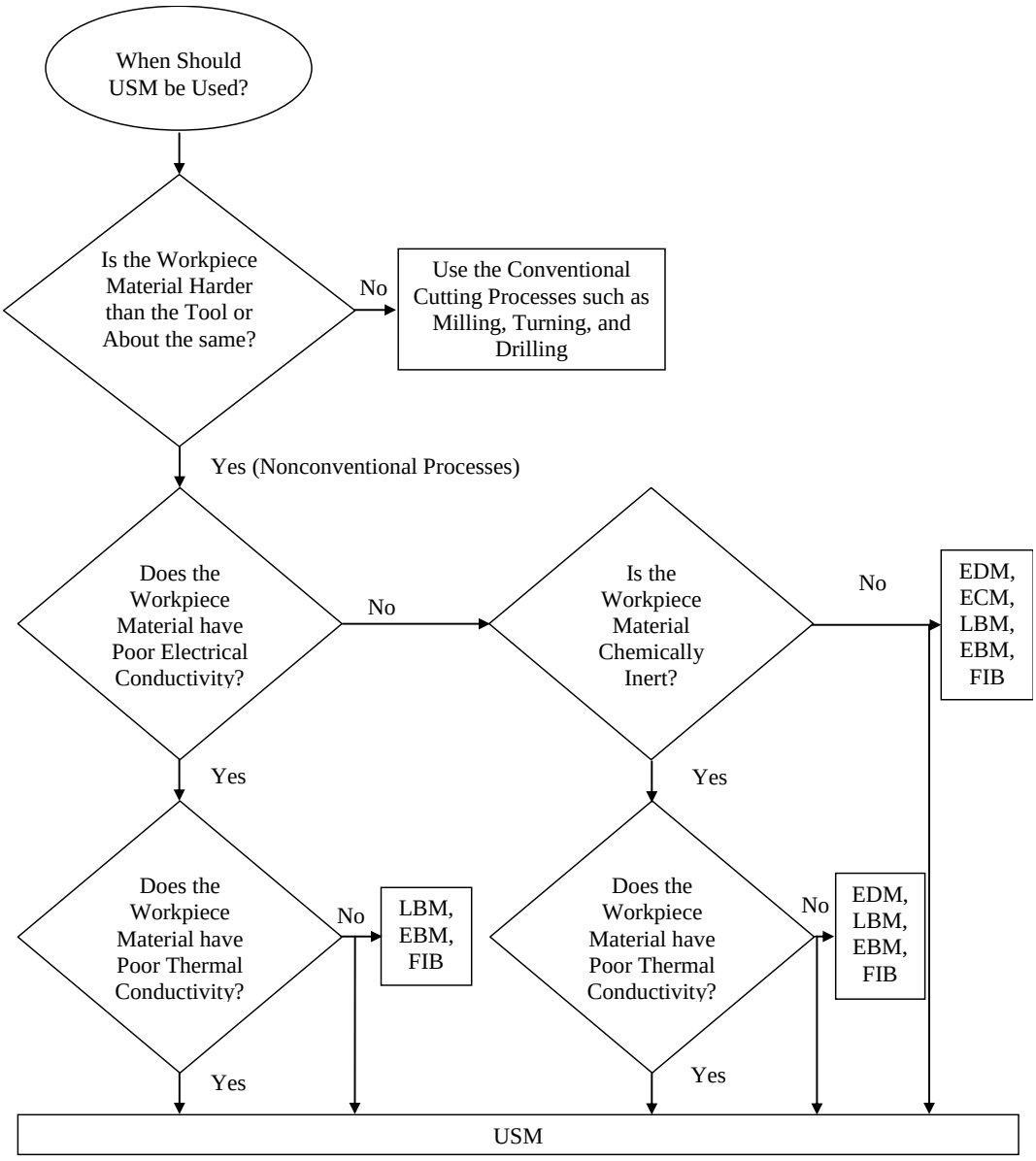

Figure 1. 1: Machining process selection flow diagram

EDM: Electrical Discharge Machining, ECM: Electrochemical Machining, LBM: Laser Beam Machining, FIB: Focused Ions Beam Machining, EBM: Electron Beam Machining, USM: Ultrasonic Machining.

1.3 Research Motivation and Thesis Objectives

Many research groups have recently developed micro USM systems to characterize the USM process at the micro level. However, the goal of this thesis is to stabilize the micro USM process in order to commercialize the process.

The cutting force variations were observed to greatly influence the machining stability and characteristics of the micro USM. Therefore, the objectives of this thesis are to:

1- reduce the cutting force variations of the micro USM process in order to utilize the cutting force as a process control parameter.
2- select the best control strategy that can be implemented to develop a robust micro USM cutting force controller.
3- study the effect of the micro USM cutting force stability on the repeatability of the micro USM process machining characteristics such as the machining rate and the surface quality.

To improve the system stability and provide better cutting force control, the following tasks need to be achieved:

1- Redesign the micro USM system to minimize the other sources of the cutting force variations such as the low cutting force sampling and servo control frequencies.
2- Improve the design of the micro USM control system to reduce the cutting force variations.

1.4 Thesis Organization

Chapter 2 consists of a literature review describing the micro USM process principle, material removal mechanism, parameters, capabilities, and recent research on the micro USM process and machine tool design.

Chapter 3 describes the Generation II micro USM system and the newly proposed micro USM system (Generation III) to achieve better cutting force control.

Chapter 4 describes the process of developing a stochastic dynamic model of micro USM cutting force using the system identification techniques.

Chapter 5 describes the results of implementing different cutting force controllers to stabilize the micro USM cutting force and the effects of these controllers on the repeatability of the machining characteristics.

Chapter 6 summarizes the conclusions and the future work recommendations.

CHAPTER 2

LITERATURE REVIEW

2.1 Introduction

The micro USM process principle, material removal mechanism, capabilities, machine tool design, and research issues are examined and summarized in this chapter.

2.2 USM Process Principle

USM is an abrasive machining process in which the material is removed from the workpiece because of the presence of abrasive particles in the machining gap, and an ultrasonically vibrating tool. Figure 2.1 shows the interactions among the tool, abrasive particles, and the workpiece that cause the material to chip away from both the tool (tool wear) and the workpiece (machined feature). Small portions of the workpiece and the tool are chipped away because of the abrasive particles indentations on the workpiece and tool surfaces at each vibration cycle. The applied cutting force and the ultrasonic vibration generate the compression stresses needed for the abrasive cutting process. The abrasive slurry supply system helps in supplying fresh abrasive particles and flushing away the debris and the old crushed abrasive particles from the machining gap. The machine feature has a negative tool shape with larger dimensions depending on the machining gap size. The principle of the material removal of the micro USM is similar to the macro USM with modifications (vibrating the workpiece instead of the tool, mainly, since it is difficult to vibrate and rotate the micro tool at the same time) to precisely remove less unit volume.

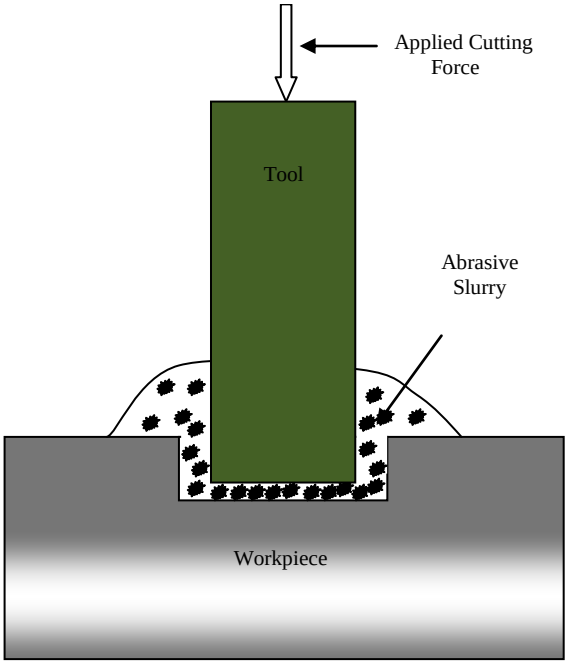

Figure 2. 1: USM process principle (tool-abrasives-workpiece interactions)

2.3 Material Removal Mechanism

In the USM, abrasive particles with random shapes and sizes are present in the machining gap between the tool and the workpiece. At each vibration cycle, the workpiece, in macro USM, or the tool, in micro USM, is displaced upward and downward causing each abrasive particle to interact with the workpiece in one of the following ways [1]:

1- Direct impact of the abrasive particles on the workpiece surface: this is common when the abrasive particle size is larger than the machining gap.

2- Impact of free-moving abrasive particles on the workpiece surface: this is common when the abrasive particle size is smaller than the machining gap.

3- Cavitations effect erosion: the high frequency vibration power generates a high frequency mechanical pressure in the slurry medium causing the abrasive particles to impact the workpiece surface.

The abrasive particles size and its random size distribution, applied cutting force, vibration amplitude, and abrasive slurry concentration are the key factors that influence the machining gap between the tool and the workpiece. Based on the machining gap, each abrasive particle could have different interaction forms, as listed above, with the workpiece. Moreover, each abrasive particle has a different penetration depth on the workpiece surfaces depending upon the abrasive particle size and shape, even under the same machining conditions.

If the applied compression pressure by the abrasive particle is low (the resulted strain is lower than the brittle fracture strain), the abrasive particle tends to remove the material from the workpiece by plastic deformation (ductile mode material fracture). On the other hand, if the applied compression pressure by the abrasive particle is high (the resulted strain is higher than the brittle fracture strain), the abrasive particle tends to remove the material by cracking the workpiece (brittle mode material fracture). The larger the abrasive particle size, the larger the compression pressure applied by the abrasive particle on the workpiece (higher effective applied cutting force) even under the same cutting force. The larger the cutting force applied on the tool, the higher the possibility that a brittle mode fracture will occur. Therefore, the material removal fracture mechanism mode of the USM process depends mainly on the applied cutting force and abrasive particles' size, size random distribution, and geometry.

Figure 2.2 shows the different material removal fracture mechanisms resulting from the effective applied pressure and the stochastic nature on the abrasive particles size and shape [2]. The brittle fracture mode is the most common fracture mode that causes the material to be removed from the workpiece in the USM process. Because of the stochastic nature of the abrasive particles and the applied cutting force variations, both the ductile and the brittle fracture modes could happen at the same time.

The brittle fracture mechanism, based on the scheme of vent crack formation with the load increasing and decreasing during the impact cycle, is illustrated in Figure 2.3. The process of cracking the workpiece material starts by crack initiation, crack generation, and then crack prorogation. The crack initiation and generation stages happen during the loading cycle (compression pressure increasing cycle (+P)); while the crack prorogation stage happens during the unloading cycle (pressure decreasing cycle (-P)).

The USM material removal mechanism was observed to be the same for the macro and micro levels. At the micro level USM, the stochastic nature of the abrasive particle size and distribution was found to have a tremendous effect on the material removal process stability [3]. It was also found that both brittle and ductile fracture modes were observed under different machining conditions; sometimes both modes were observed together under the same machining conditions [3]. Therefore, the prediction of the micro USM process material removal mechanism was difficult.

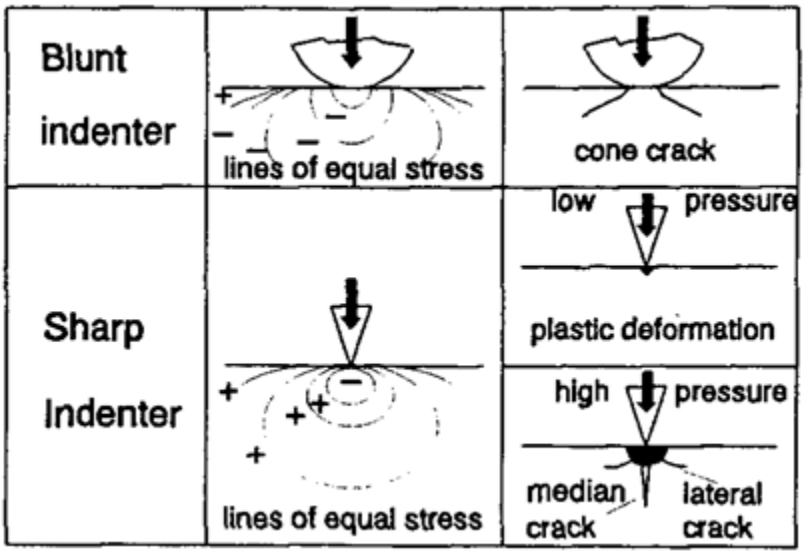

Figure 2. 2: Localized fracture of brittle materials by single abrasive particle [2]

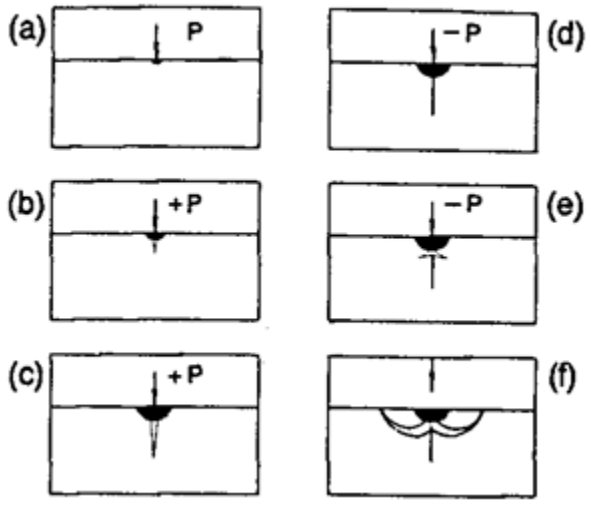

Figure 2. 3: Scheme of the vent crack formation [2]

2.4 Micro USM Process Parameters

The abrasive slurry parameters (abrasive particle size, slurry concentration, and slurry medium), ultrasonic vibration parameters (vibration amplitude and frequency), cutting force, and workpiece and tool material properties are the key parameters that influence the micro USM process performance as illustrated in Figure 2.4. The main machining performance measures are the process productivity (machining rate) and the machined features quality (surface finish and dimensional accuracy). The effects of these parameters on the micro USM machining performance have been recently investigated. The effects of these machining parameters on the machining performance of micro USM process are summarized as followings:

1- Abrasive Particle Size

The larger abrasive particle was found to give higher machining rates [4]. For the same machining conditions, different abrasive particle sizes led to different fracture mechanisms and a transition between both the brittle and the ductile modes [5]. The surface roughness was decreased when small abrasive particle size was used [6].

2- Abrasive Slurry Medium

Using aqueous based slurry, the machining rates and the machined features surface roughness were increased compared to that of the oil based slurry. Using the oil based slurry, three body material removal mechanisms were found to dominate the material removal mechanism compared to two body material removal mechanisms using aqueous based slurry [7].

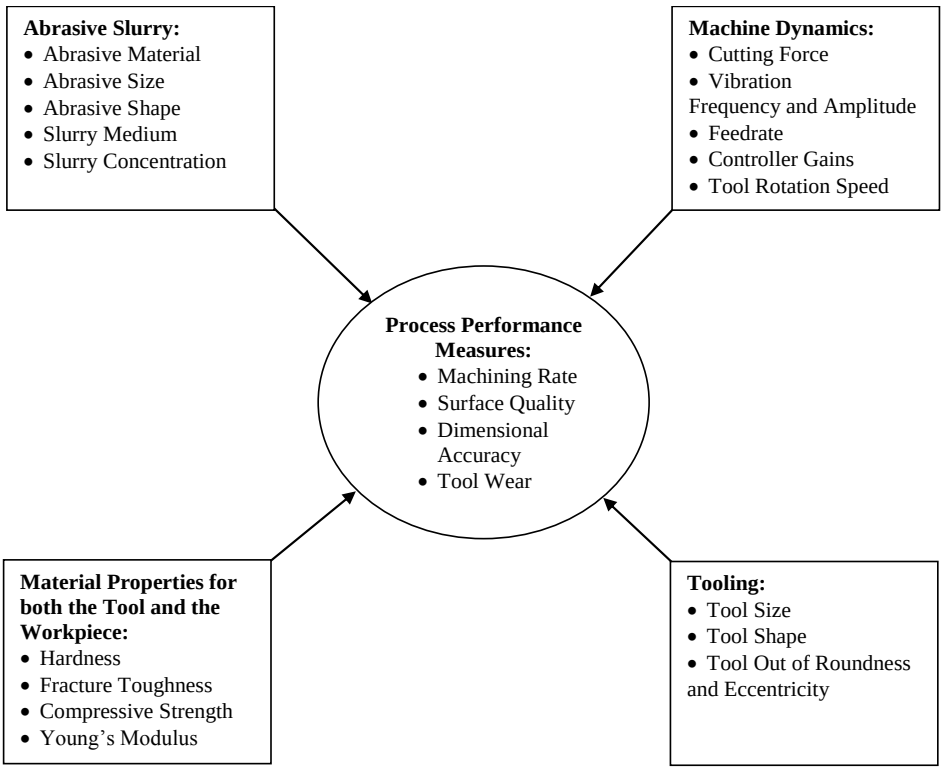

Figure 2. 4: Micro USM process parameters and performance measures

3- Abrasive Slurry Concentration

The slurry concentration was found to have an insignificant effect on the machining rate and the machined surfaces roughness [7].This is mainly because it was hard to maintain the slurry concentration constant because of the fluid evaporation and mist caused by the ultrasonic transducer's temperature increase and ultrasonic vibration, respectively.

4- Cutting Force (Static Load)

The higher cutting force value led to an increase in the machining rates until certain ranges where the machining rate started dropping because of the abrasive particles crushing and inefficient slurry flushing [8][3].

5- Tool Rotation

Implementing the tool rotation was found not to improve the machining rate [3]. However, it helps in leveling out the bottom of the machined holes.

6- Material Fracture Toughness

The machining rate was found to increase when the workpiece material fracture toughness decreases [5].

7- Vibration Amplitude

The machine rate was increased with the increase of the vibration amplitude. When the vibration amplitude approaches the abrasive particle size, the best performance in terms of the machining rates and the surfaces quality of machined features was obtained [4].

A theoretical model was developed to analyze the effect of the key micro USM parameters (vibration frequency and amplitude, abrasive particle size, workpiece material properties, slurry concentration, and cutting force) on the machining rate analytically using the same assumptions used to model the machining rate in the Rotary Ultrasonic Machining (RUM) process [8].

2.5 Micro USM Process Capabilities

Micro USM was applied to machine micro features in several hard and brittle workpiece materials such as quartz [9], glass [10], silicon [11], and alumina [12]. Using the micro USM, both the die sinking mode (2D die profile or multi-cylindrical-tool die for multi-hole drilling) and the tool path generation mode (using cylindrical tool shape)

were used to machine complex features. The shapes varied from simple holes to 3D complex cavities that were machined in several hard and brittle materials. Table 2.1 summarizes the micro USM shapes that were machined using the micro USM process. High aspect ratio features (1:10) were achieved in hard and brittle materials using the micro USM process. Several holes, as small as 5 µm in diameter, were machined in quartz, glass, and silicon using a 4 µm diameter tungsten carbide tool [9]. Moreover, low surface roughness, down to Ra = 0.2 µm, was achieved under optimized machining conditions [7].

Table 2. 1: Micro USM process capabilities

Dimension	Feature	Tool Shape	Materials	Reference
1D	Holes	Cylindrical	Tool: Tungsten W/P: Silicon	[9]
	Multi-Holes	Array of Cylindrical Tools	Tool: PCD W/P:Glass	[13]
2D	Multi-Spiral Channels	Cylindrical	Tool: PCD W/P:Sillicon	[14]
	Gears and Racks	Die sinking	Tool: Tungsten W/P: Alumina	[12]
3D	3D Free Form Cavity	Cylindrical	Tool: Tungsten W/P: Silicon	[11]

2.6 Micro USM Machine Tool Design

The process parameters controls of the micro USM process should first be modified to reduce the energy released at each vibration cycle to precisely control the removed unit volume. Table 2.2 shows a comparison of the key control parameters ranges for the USM process at both the macro and the micro levels. The accuracy and capability of macro USM machines were not suitable to achieve these control parameters ranges at the micro level. Therefore, designing a micro USM system was essential to improve the system positioning accuracy, improve the cutting force control accuracy and repeatability, and reduce the vibration amplitudes. Since the micro USM process is still in the research stage, many groups designed different micro USM machines to achieve these control parameters [15][11][14]. Table 2.3 summarizes the different micro systems designs issues and modifications that were proposed to address these issues. The advantages and the disadvantages of implementing these innovations on the micro USM system's performance are also listed.

Table 2. 2: Macro USM vs micro USM process parameters [3]

Parameters	**Macro USM**	**Micro USM**
Vibration frequency	Around 20 KHz	Above 20 kHz (40 KHz is commonly used frequency)
Vibration amplitude	Tens of microns (8~30 μm)	Within microns (0.5~5 μm)
Abrasive particle size	Tens of microns (50~300 μm)	Within microns (0.5~5 μm)
Cutting force (static load)	In range of kilogram-force	In range of gram-force

Table 2. 3: Micro USM systems design issues and modifications

Modification	Motivation	Advantages	Disadvantages
Improve the system accuracy (high precision stages) [16]	▪ Precision motion control ▪ Control the removed unit volume	▪ Better process control ▪ Better cutting force control	▪ Expensive ▪ Stages misalignment
Application of tool rotation [16]	▪ Minimize the holes out-of-roundness error caused by the tool misalignment	▪ Stir the slurry to supply fresh abrasive and remove debris ▪ Reduce the tool misalignment effect on the hole perpendicularity	▪ Difficult to vibrate the tool ▪ High cutting force variations ▪ Larger the holes diameter for the same tool
On-the-machine tool preparation [15]	▪ Reduce the tool holding and mounting error	▪ Easy tool changing and holding ▪ Reduce installation errors	▪ Add more complexity to the system design
Appling the ultrasonic vibration to workpiece instead of the tool [9]	▪ Obtain high accuracy tool rotation (it is hard to vibrate the tool while it rotates)	▪ Using universal accurate spindle is possible (vibration is not needed) ▪ Improve the debris removal and slurry refreshment ▪ Easy to design system ▪ ability to load/unload the tool after perpetration	▪ Difficult to extend the machine for 5-axis machining ▪ Hard to design slurry tank or circulation mechanism (change resonant frequency of the PZT transducer) ▪ Poor workpiece holding ▪ Slurry medium evaporation and mist due to the generated heat and vibration of the transducer
Use electroheological slurry medium with magnetic field between the tool and the workpiece [17]	▪ Push fresh abrasive particles to enter the machining gap	▪ Improve the machining rate ▪ Improve the process stability	▪ Add more complexity to the design
Tool feed control using the Acoustic Emission (AE) signal [14]	▪ Prevent the tool breakage and bending	▪ Facilitate the engagement between the tool and workpiece ▪ Using the online tool wear compensation	▪ Need more effort to design and implement ▪ The AE signal has no physical meaning ▪ Different AE signal levels at different workpiece positions
Milli force measurement and control using voice-coil as actuator and force sensor [18]	▪ Improve the cutting force measurement accuracy	▪ No need to use load cell or dynameters for cutting force measurements	▪ Need more effort for design and implementation ▪ Expansive equipment

2.7 Limitations and Research Issues

2.7.1 Tool Wear and Breakage

The applied load interactions with the abrasive particles in the machining wear both the tool and the workpiece. The ratio of material removed from the tool to that of the workpiece should be kept to a minimum. The tool material hardness and fracture toughness are the major two material properties that influence the tool wear rate. The harder the tool material, the lower the tool wear rate. For example, a sintered diamond tool was found to be the best tool material in terms of reducing the tool wear rate [9]. A viscoelastic thermoplastic tool was also effectively used to reduce the tool wear rate in the micro USM process [19]. The tool wear rate was found to be higher for the smaller tool diameter [16]. The tool wear rate increases with the increase of the vibration amplitude and abrasive particles size [9][20]. The tool wear rate was also increased with the increases of the cutting force or the feed rate in both constant forces and constant federate modes, respectively [20]. The tool tip wear shape was observed to be spherical after some machining [21]. The longitudinal tool wear compensation was essential to produce 2D and 3D features with a consistent depth. Therefore, a “Uniform Tool Wear” method was proposed to compensate for the longitudinal tool wear rate during the micro USM process. A 3D free form cavity was successfully machined on a silicon workpiece using the proposed method as shown in Figure 2.5 [11]. Moreover, The Acoustic Emission (AE) RMS signal was also used to compensate for the longitudinal tool wear rate of the micro USM process by controlling the AE signal level constant during machining [14].

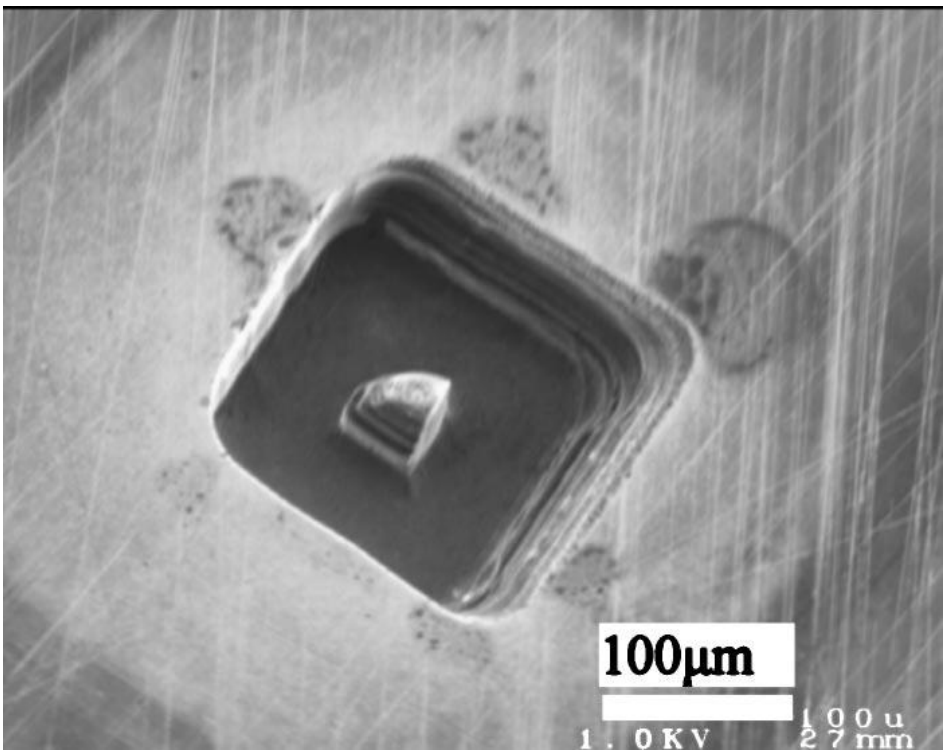

Figure 2. 5: 3D machined feature using the " Uniform Tool Wear" method [11]

The dynamic stability of the micro USM tool under the compression load was modeled to prevent tool breakage and bending. A method to determine the critical tool length based on the generated stresses was proposed to prevent the tool breakage and bending during machining [22].

2.7.2 Process Repeatability and Stability

The tool rotation was found to generate radial bending moments during the tool rotation because of the tool eccentricity [22]. These forces influenced the process stability (disturbed monitoring and the control signals such as the cutting force and AE) and caused the tool breakage.

In USM, the tool feed during machining happens under either the constant cutting force mode or the constant feed rate mode. The constant cutting force mode was found to have an advantage in preventing the tool breakage in the micro USM process, even when the tool rotation was implemented [3]. It was difficult to control the cutting force variations during the machining. The cutting force variations caused instability of the machining performance, because different cutting force values were engaged in the cutting process mechanism. Therefore, the machining characteristics of the micro USM process were unrepeatable [3].

2.7.3 Debris Accumulation and Slurry Flushing

The machining rate of the micro USM process was observed to decay depending on the machining time. The debris accumulation and the abrasive particles crushing hypothesis were proposed to be the main reason for the machining rate decay. A theoretical model was developed to evaluate the ultrasonic vibration impact efficiency because of the debris accumulation in the machining gap [23]. A flushing mechanism is needed to refresh the slurry medium between the tool and the workpiece. In the micro USM, applying the slurry flushing caused tool vibration and breakage. Therefore, the micro USM cutting was usually conducted without slurry flushing. An electroheological slurry medium was used to force the abrasive particles inside the machining gap by generating a magnetic field between the tool and the workpiece (pushing fresh abrasive particles into the machining gap and removing the old abrasive particles and debris) [17].

The research issues of micro USM process can be summarized as the following:

1- Integrate the micro USM process performance such as the tool wear rate with a CAD/CAM method to create complex 3D features.
2- Improve the design, precision, capabilities, and performance of micro USM machine tools in order to commercialize the process.
3- Improve the repeatability and stability of the micro USM machining performance by using the machining gap on-line sensing, monitoring, and control techniques.
4- Model and predict the material removal mechanism of micro USM process.
5- Improve the quality of the micro machined features (dimensional accuracy mainly by reducing the machining gap).
6- Study the effect of the key process parameters on the machining characteristics.

CHAPTER 3

SYSTEM DESIGN AND EXPERIMENTAL DETAILS

3.1 Introduction

Even though the micro USM is a downscaled version of the macro USM process, using the macro USM machines to generate micro features was limited by the accuracy and the repeatability of the machining system at the micro level. The micro USM system includes similar system components as those used in the macro USM system. The components' specifications were adapted to precisely remove lower unit volume per vibration cycle at the micro level machining. Recently, an in-house-built micro USM system was developed in the Center for Nontraditional Manufacturing Research (CNMR) at the University of Nebraska-Lincoln to investigate the USM process characteristics at the micro level. In this chapter, the micro USM system design is described and a new system is proposed to satisfy the requirements of implementing a better cutting force control.

3.2 Micro USM Systems Structure

Some changes were introduced to the USM systems design at the micro level. The micro USM machining system was similar to the macro USM machines in the topology and the structure. Figure 3.1 shows a commonly adapted micro USM system structure schematic that was used by many research groups to build a micro USM machining system.

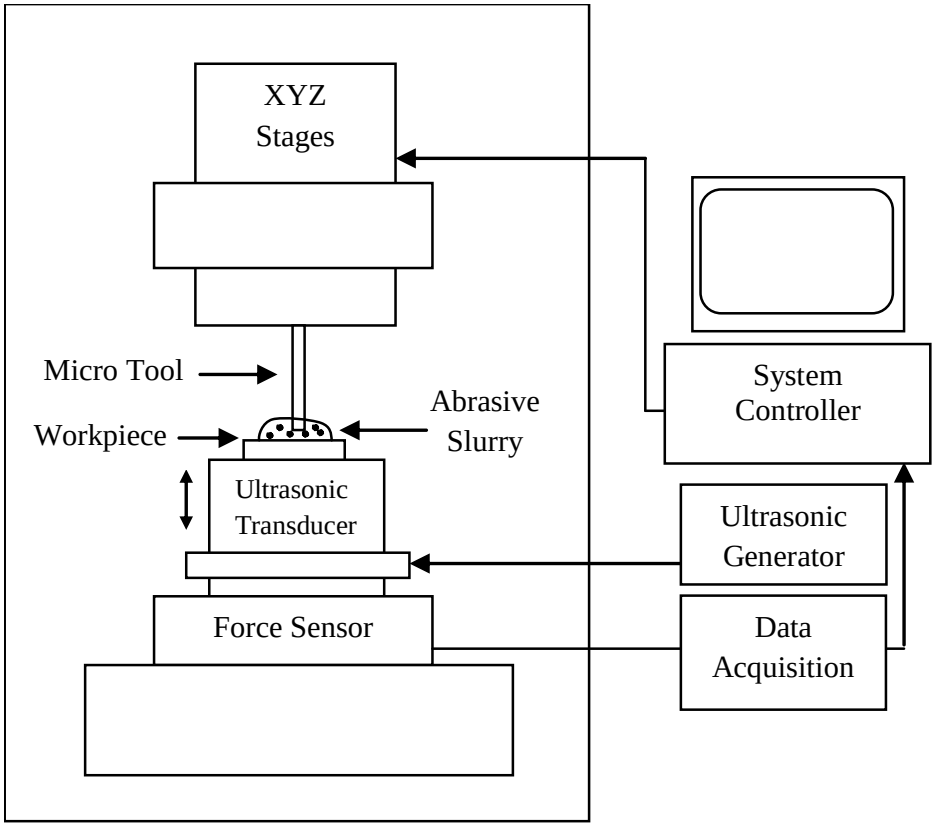

Figure 3. 1: Micro USM system structure

The following is the list of the basic components required to build a micro USM system:

1- Ultrasonic vibration system (transducer and generator)

2- Positioning stages (XYZ-stages)

3- Cutting force feedback sensor

4- System controller

5- Machine spindle

6- Tool holder

7- Workpiece holder

3.3 Generation II Micro USM System Description

Figure 3.2 shows the Generation II micro USM system experimental setup, which was previously developed at the CNMR. The basic system components that were used to develop this micro USM experimental setup are the following:

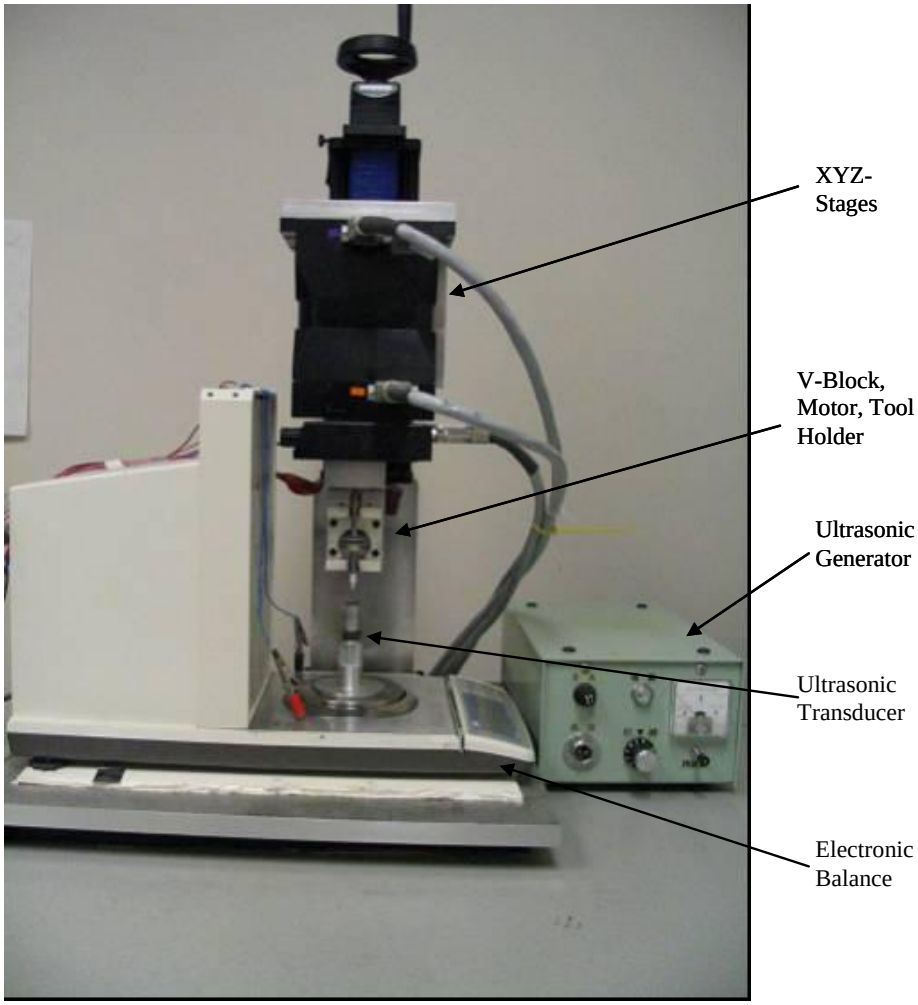

Figure 3. 2: Generation II micro USM system experimental setup

1- Ultrasonic Vibration Unit

A Piezoelectric (PZT) transducer (Model DA21540F, NGK Spark Plug Co., Ltd.) with 39.5 ± 1 KHz resonant frequency was used to ultrasonically vibrate the workpiece. A high frequency electrical signal was provided using an analog ultrasonic generator (Model GT-100, NGK Spark Plug Co., Ltd.). The ultrasonic generator converts the regular low frequency electrical signal to an ultrasonic frequency voltage signal (~40 KHz). The voltage signal level was used to control the vibration amplitude of the PZT actuator; the applied voltage signal value is linearly proportional to the vibration amplitude.

2- Driving Stages (XYZ-Stages)

High precision XYZ-stages (Model PM500-XYZL, Newport Co.) with ± 0.025 μm resolution and ± 0.1 μm repeatability were used to control the tool position and the tool feed rate during machining. A compatible motion controller (Model PM500-C6, Newport Co.) with 200 Hz servo frequency was used to drive the stages.

3- Force Measurement Sensor

An electronic balance (Model HM-200, A&D Co. Ltd.) with ± 0.001 gf resolution was installed to sense the cutting force applied between the tool and the workpiece. A serial communication port (RS-232) was used to read the cutting force signal at 5 Hz frequency.

4- System Controller

A LabVIEW PC-based controller was designed, implemented, and tested several times to ensure constant cutting force control. The communication between the LabVIEW PC-based controller with the Newport controller and the electronic balance was performed through a standard parallel port, and a serial port (RS-232), respectively. At each control cycle, the LabVIEW controller compares the reference force set point with the actual cutting force signal and adjusts the Z-axis stage position to maintain constant cutting force.

5- Tool Holder

A high precision V-Block bearing, which was originally used as a tool holder and a tool rotation guide for micro EDM machine (Model MG-ED 72W, Panasonic Co.), was utilized to hold the tool and provide a precision rotational guide for the micro USM system. Because the micro USM tools were prepared using the Micro Electrical Discharge Grinding (Micro WEDG) unit on the micro EDM machine where the V-Block was utilized as a tool holder, using the V-Block bearing as a tool holder for the micro USM system was convenient to eliminate the issues of the tool eccentricity, holding, and interchange. A precision coreless micro DC motor (LN22, Canon Precision Inc.) was installed to rotate the tool and control the tool rotational speed using a standard laboratory digital power supply (the rotational speed of the tool is linearly proportional to the applied voltage signal level on the DC motor).

6- Workpiece Holder

Adding an additional weight above the PZT transducer was observed to change the transducer resonant frequency. Therefore, double sided tape was used to hold the workpiece on the PZT transducer without changing the transducer resonant frequency (the weight of the workpiece usually is less than 1 gf and doesn't affect the transducer resonant significantly).

3.4 Generation II Micro USM System Limitations

The electronic balance (± 0.001 gf resolution and 5 Hz sampling frequency) was utilized as a feedback sensor of the cutting force during machining. The resolution of this feedback sensor was enough, compared to the lowest used cutting force value (2 gf). However, the sampling rate of the electronic balance (5 Hz) was very slow compared to the Z-axis stage's servo frequency (200 Hz). The slow feedback response signal of the electronic balance limited the implementation of a faster cutting force control. Moreover, the data communication between the electronic balance and the PC-based controller had a 0.2 second time delay (limited by the electronic balance sampling rate). Therefore, a faster feedback cutting force measurement sensor was necessary to provide more detailed data about the cutting force dynamics and the machining gap state during machining.

3.5 Newly Designed (Generation III) Micro USM System

To achieve better cutting force sampling and servo control frequencies, the electronic balance was replaced by a miniature load cell (Model 31, Honeywell Inc.) with 700 Hz natural frequency and ± 0.15 gf resolution. The new load cell output force signal was amplified using an in-line amplifier (UV Model, Honeywell Inc) with ± 5 V output

voltage range and 100 Hz anti-aliasing filter. The in-line amplifier was used to amplify the load cell output signal and filter the high frequency noises. A Data Acquisition (DAQ) card with 200k samples/second and 16-bit resolution was used to sample the raw cutting force signal (batch sampling rate of 40 Hz, and 10 samples per batch). A higher sampling rate could be achieved using this load cell, amplifier, and DAQ board. However, the system sampling rate was limited by the real time sampling capabilities of the PC-based LabVIEW software. To reduce the measurement noise level, The Root-Mean-Square (RMS) value was calculated for each ten samples in the same batch. The RMS value was then utilized as a feedback signal for the cutting force control algorithms. Therefore, the frequency of 40 Hz was used as a real time servo control frequency.

The system design was modified to install the new load cell. The final system servo control frequency was eight times faster than the Generation II system. Figure 3.3 shows the Generation III micro USM system experimental setup.

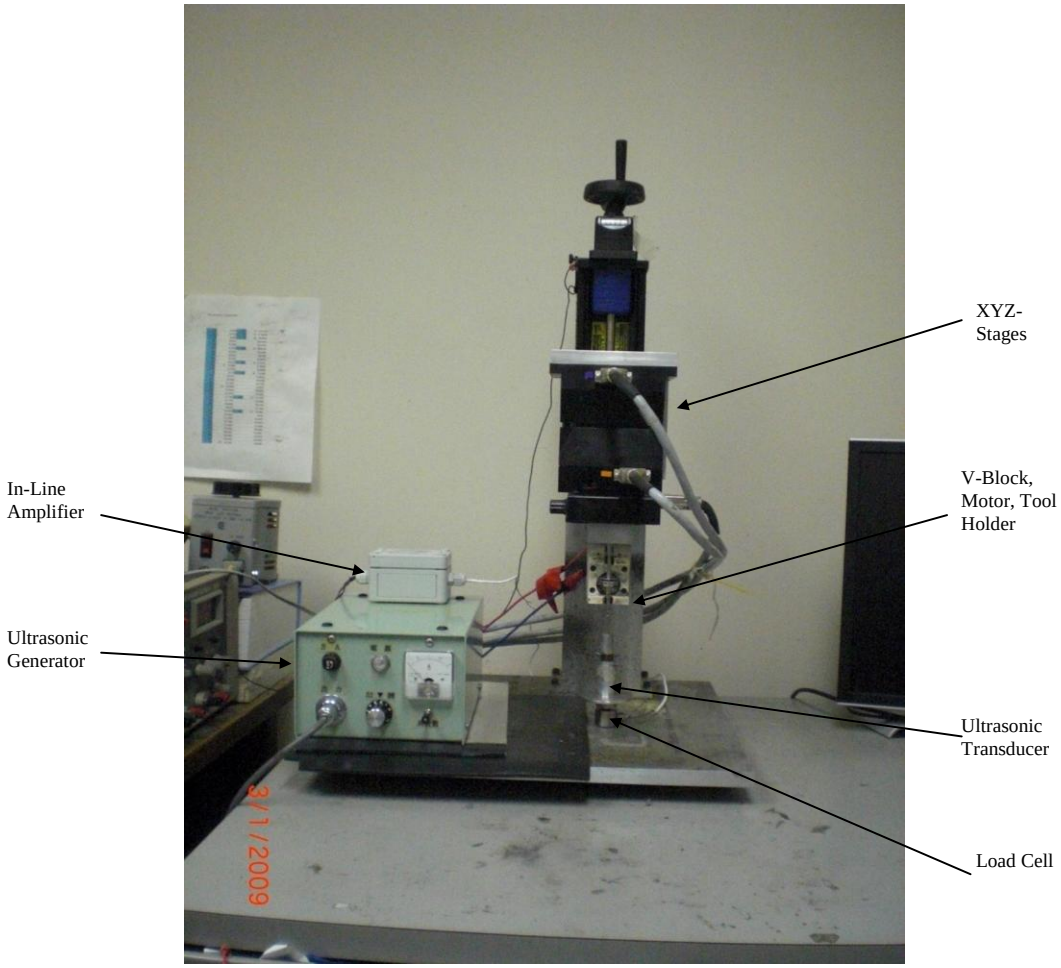

Figure 3. 3: Generation III micro USM system experimental setup

3.6 System Comparison (Generation II vs III Systems)

The cutting force responses for the Generation II and the Generation III systems under the Proportional (P) controller with Proportional Gain (K_p) = 0.1 and 5 gf cutting force set point are shown in Figure 3.4. The Generation III system showed a faster cutting force response and reduced the cutting force overshoot compared to the Generation II system because of the faster cutting force sampling and servo control frequencies.

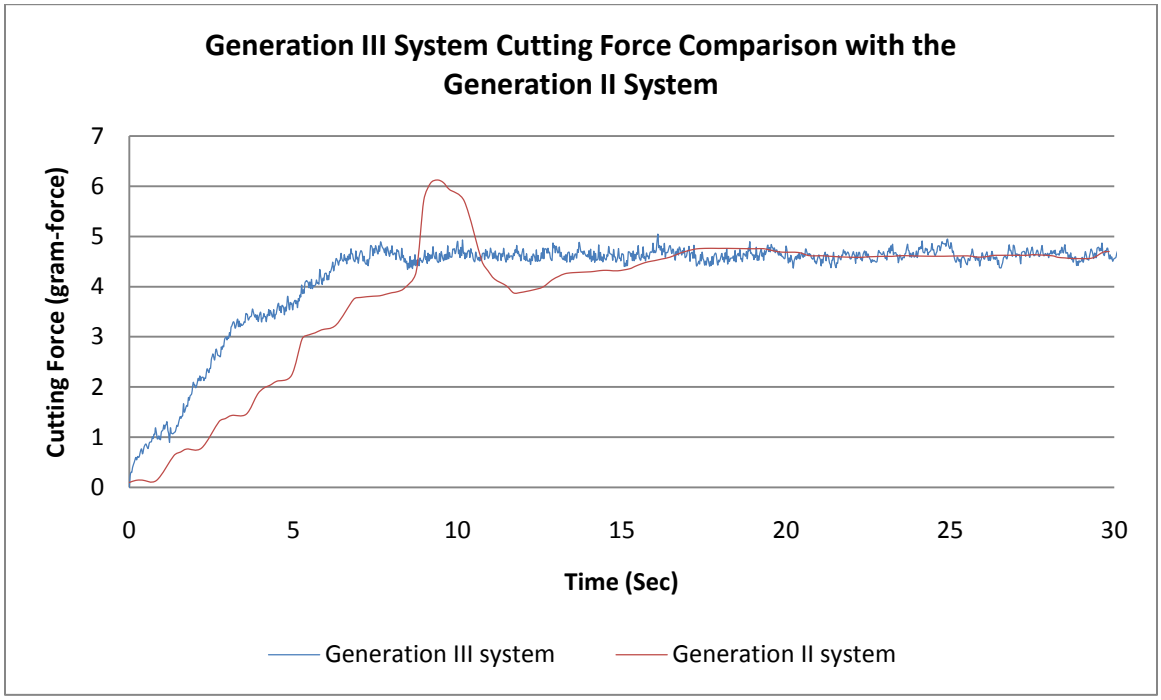

Figure 3. 4: Generation II system (5 Hz servo frequency) vs Generation III system (40 Hz servo frequency) cutting force responses (K_p = 0.1, 5 gf cutting force, no tool rotation, 1-3 µm abrasive particles size, 5% abrasive slurry concentration, 1 µm vibration amplitude)

Both systems' performances were also compared based on the machined surface quality and the machining rate. The surface roughness of the hole that was machined using the Generation III system (Ra = 0.26 µm) was less than the Generation II system hole surface roughness (Ra = 0.32 µm). Figure 3.5 shows two holes machined under the same machining condition using both systems. The Generation III system shows a slight improvement in the machining rate compared to Generation II system as shown in Figure 3.6. These improvements in the machining characteristics are related to the increase of the cutting force sampling and servo control frequencies.

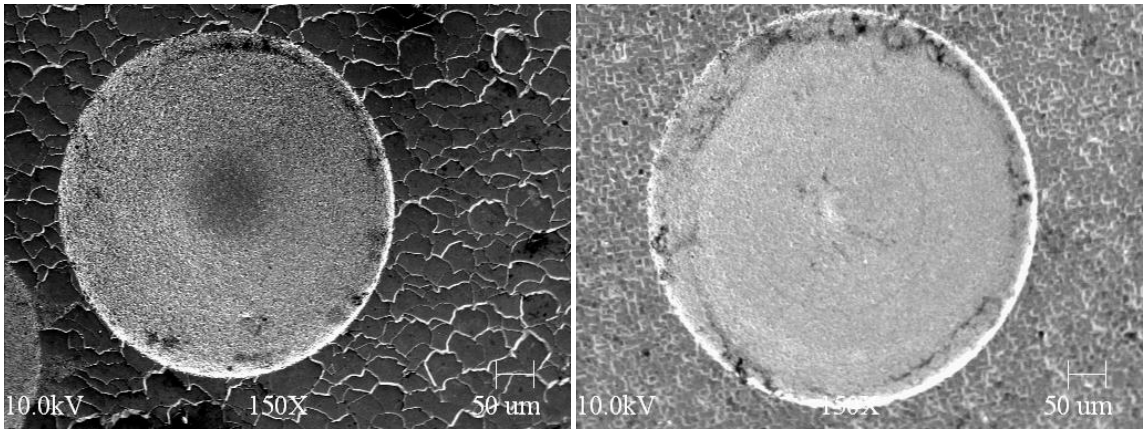

(a) (b)

Figure 3. 5: SEM pictures for the Generation II system (a) vs the Generation III system (b) machined holes under the same machining conditions (K_p = 0.1, 5 gf cutting force, 5000 rpm tool rotation speed, 1-3 µm abrasive particles size, 5% abrasive slurry concentration, 1 µm vibration amplitude)

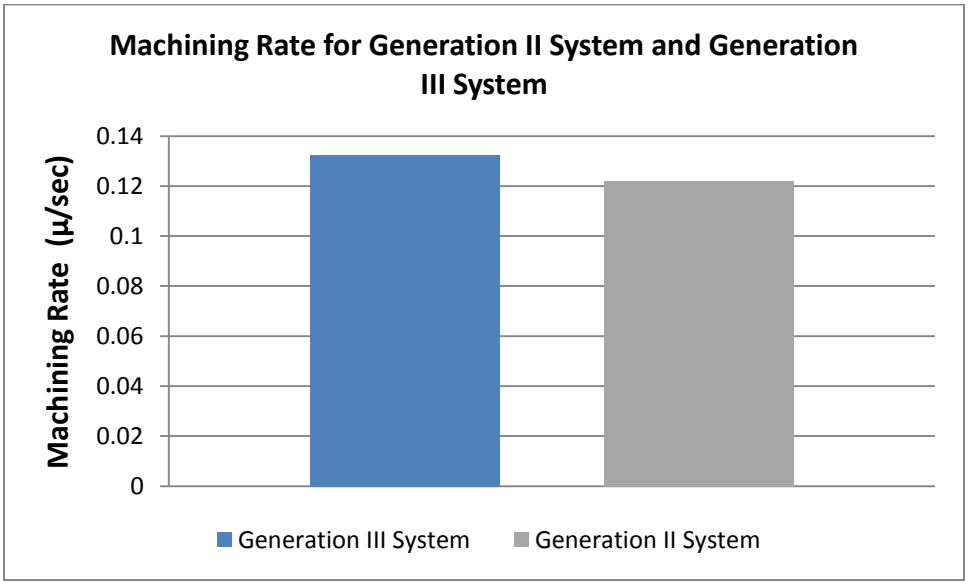

Figure 3. 6: Machining rates for Generation II system vs the Generation III system machined holes under the same machining conditions (K_p = 0.1, 5 gf cutting force, 5000 rpm tool rotation speed, 1-3 µm abrasive particles size, 5% abrasive slurry concentration, 1 µm vibration amplitude)

3.7 Generation III System Issues

The cutting force variations under the Generation III system were observed to be high when the tool rotation was employed. Because the Generation III system load cell stiffness was higher compared to the Generation II system, the effect of the tool eccentricity during rotation was higher. The tool eccentricity displaced the tool in the radial directions generating a bending moments in all directions. The effect of these bending moments appears as cutting force variations using the axial load cell measurement device. Figure 3.7 shows the difference in the cutting force variations for the Generation III system using the tool rotation (~ ± 1 gf) and without using the tool rotation (~ ± 0.25 gf). The Generation III system was more sensitive to the tool eccentricity, because the load cell sensor stiffness is higher than the stiffness of the electronic balance used in the Generation II system (more force measurement value for the same displacement value caused by the tool eccentricity). The main advantage of implementing the tool rotation was to level out the machined holes' bottoms and stir the abrasive slurry [3]. For example, Figure 3.8 shows the tool rotation effect on the machining rate. The results show that the tool rotation has an insignificant effect on the machining rate. Therefore, the rest of the experiments for the cutting force modeling (Chapter 4) and the controller design (Chapter 5) were conducted without the tool rotation to eliminate the effect of the tool eccentricity on the cutting force signal.

Moreover, the Generation III system load cell cutting force sensor accuracy and repeatability (± 0.15 gf) was lower than the Generation II system (± 0.001 gf). Therefore, the measurements noise were higher for the Generation III system even after calculating

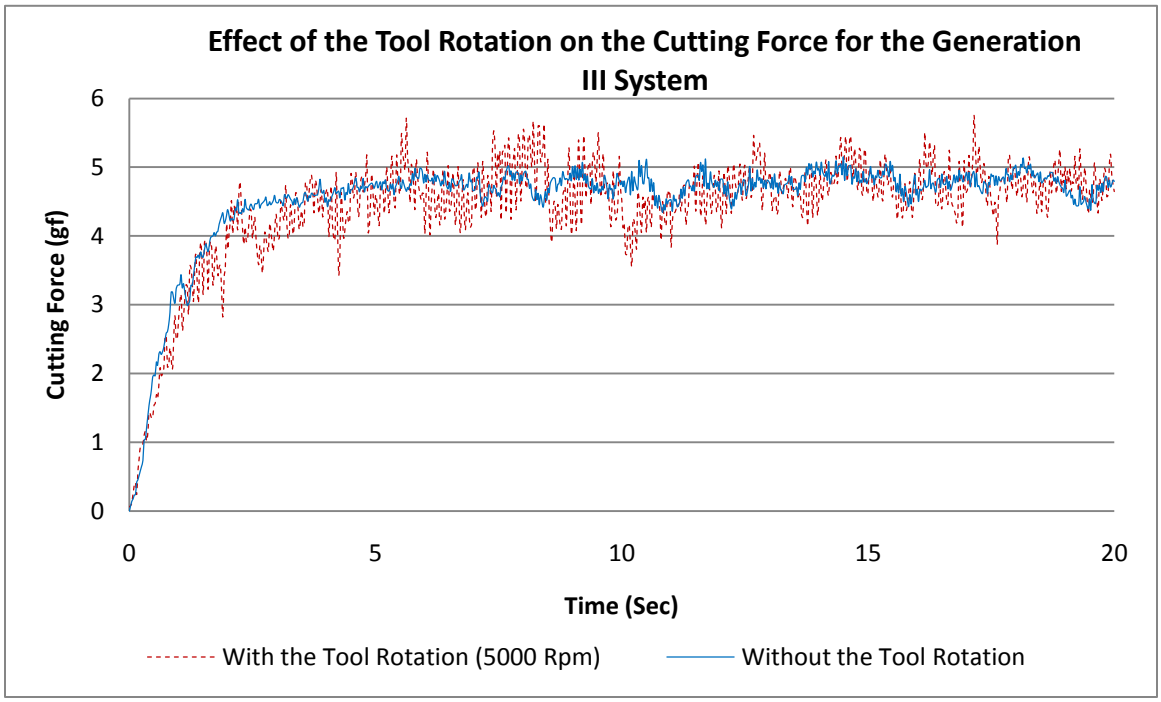

Figure 3. 7: Effect of the tool rotation on the cutting force for the Generation III system (K_p = 0.375, 5 gf cutting force, 1-3 µm abrasive particles size, 5% abrasive slurry concentration, 1 µm vibration amplitude)

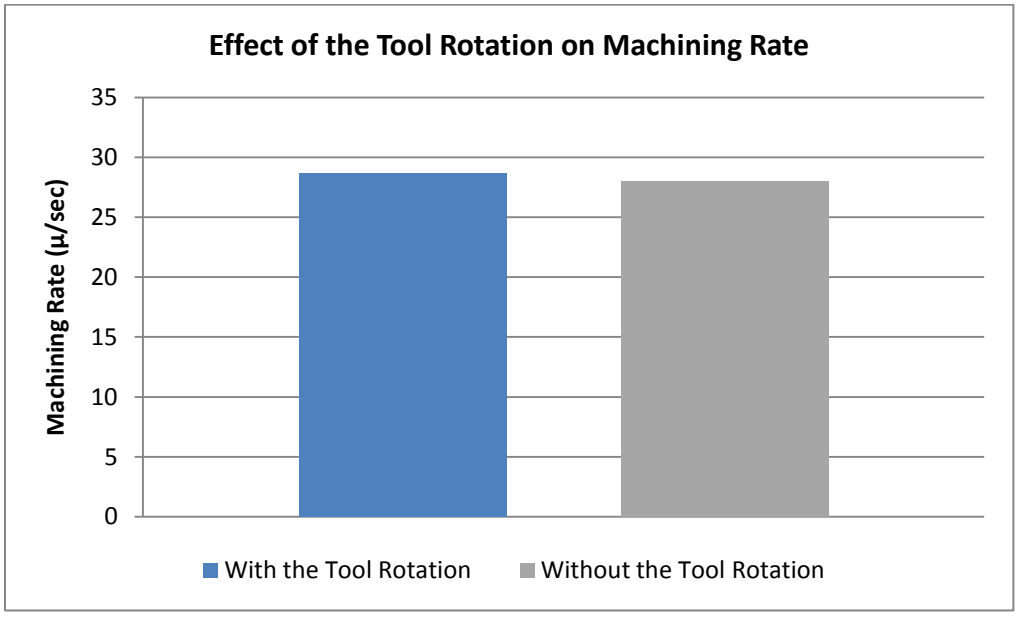

Figure 3. 8: Effect of the tool rotation on machining rate for the Generation III system (K_p = 0.375, 5 gf cutting force, 0 or 5000 Rpm tool rotation)

the RMS value (works as low pass filter for the measurements noise). Figure 3.4 also shows the effect of the high frequency measurements noise on the cutting force response of the Generation III system compared to the Generation II system cutting force responses.

3.8 Machining Conditions of Micro USM Experiments

Table 3.1 summarizes the experiential conditions of the Generation III micro USM system that was used for the cutting force modeling (Chapter 4) and the cutting force control system design (Chapter 5). Large abrasive particles (1-3 μm) were used for these experiments to demonstrate the highest variations of cutting force and machining characteristics as reported in [3].

Table 3. 1: Machining conditions for micro USM experiments

Vibration frequency	39.5 kHz
Vibration amplitude	1 μm
Abrasive particle material	Polycrystalline diamond (PCD)
Abrasive particle size	1-3 μm
Abrasive particle concentration	5 % by weight to water
Tool material	Tungsten
Tool diameter	300 μm
Workpiece material	Silicon <111>
Tool Rotational Speed	0 Rpm

CHAPTER 4

DYNAMIC MODELING OF MICRO USM CUTTING FORCE

4.1 Introduction

In the previous chapter, the micro USM system design was modified to achieve faster cutting force sampling and servo control frequencies. The achieved frequencies show an improvement on the micro USM cutting force control under the P controller; however, a better cutting force controller can be designed. Therefore, a dynamic model of the micro USM cutting force was essential to understand the dynamics behavior of the system and to design a better cutting force controller. The micro USM process is a highly stochastic process. Therefore, the model of the cutting force dynamics should account for both the deterministic and the stochastic nature of the system dynamics. In this chapter, the process of developing a dynamic model for the micro USM cutting force is described.

4.2 Dynamic Systems Modeling

The process of designing a control system for any dynamic system starts by developing a dynamic model of the system, selecting the controller structures, designing the controller to simulate the system performance off-line, and finally implementing and evaluating the control system behavior on-line. Different real world systems require different controller structures depending on the system type. The systems dynamics can be classified into the following types:

1- Linear vs Nonlinear Systems

For linear dynamic systems, the change of the system output variable is linearly proportional to the change of the system input variable. The linear system response also obeys the principles of superposition and homogeneity. The linear system dynamics can be expressed using linear differential equations for continuous systems or linear difference equations for the discrete systems. The sources of systems' nonlinearity are the saturation, dead-zone, friction, backlash, quantization effects, relays and switches, and rate limiters. In general, all the real world systems include some sort of nonlinearity. However, most of the dynamic systems can be approximated as linear systems.

2- Time Variant vs Time Invariant Systems

The physical parameters of the time-invariant systems are not functions of time. The system dynamic models for linear time invariant systems behavior can be expressed using differential/difference equations with constant coefficients. Some systems have time variant parameters (e.g. the flight vehicles have variable mass depending on the flight time because of the fuel burning). The linear time variant systems dynamics can be described using linear differential/difference equations with time varying coefficients.

3- Discrete vs Continuous Systems

The continuous dynamic systems models are defined at any point of time while the discrete systems models are defined at specified moment where the data were sampled. The continuous systems dynamic model coefficients are related directly to the process physical parameters (e.g. the time constant for an RL-circuit depends on the resistant and the inductance values). The discrete dynamic systems models are widely utilized because

they are compatible with digital computers. A discrete model of the system dynamics can be obtained directly using the experimental approach.

The dynamic model of the system can be describe using differential/difference equations (either linear or nonlinear, or time variant or time invariant).Writing the equations that describe the system dynamics is the most difficult part of the systems modeling process. Many approaches were used to develop dynamic models for the dynamic systems. These methods are summarized below:

1- Physical Approach

It is also known as the white box approach. The system dynamics are described based on the physical laws that govern the system dynamics (e.g. Newton's second law of motion and conservation of energy). This approach is usually utilized for modeling simple systems dynamics, because it is easier to write the equations that describe the system dynamics analytically.

2- System Identification Approach

It is also known as the black box approach. The system dynamic model is developed without any prior knowledge about the physical laws of the system. The dynamic model of the system response is developed based on experimental data (fitting a model between the system inputs and the system outputs). This approach is usually utilized for modeling complex system dynamics, because it is difficult to write the equations that describe the system dynamics analytically.

3- Mixed Approach

It is also known as the gray box approach. Both the white box and the black box approaches are used together to build a dynamic model of the system.

4.3 System Identification Methods

Using the system identification methods, the dynamic model of any system can be estimated based on experimental data acquired from the system. The system identification methods for the linear systems can be classified into the following [24][25].

4.3.1 Nonparametric Model Estimation Methods

The frequency response function and the impulse response are the most common nonparametric system identification methods. The impulse response is usually used to provide information about the system time delay, system damping, and the system forgetting factor (system memory). The frequency response function is usually used to provide information about the system natural frequencies. Both methods are an easy way to develop a dynamic model of the system. However, the accuracy of the nonparametric model estimation methods is low compared to the parametric model estimation methods. Therefore, the nonparametric methods are always used to evaluate the system dynamics before applying the parametric model estimation methods.

4.3.2 Parametric Model Estimation Methods

The parametric model estimation methods are used to describe the systems dynamic behavior based on stimulus control U(k) and disturbance D(k) inputs. All the parametric model estimation methods are special cases from the General Linear Polynomial (GLP) model. Figure 4.1 shows the structure of the GLP model; Equation (4.1) describes the GLP model. Table 4.1 also shows all the possible parametric model estimation models.

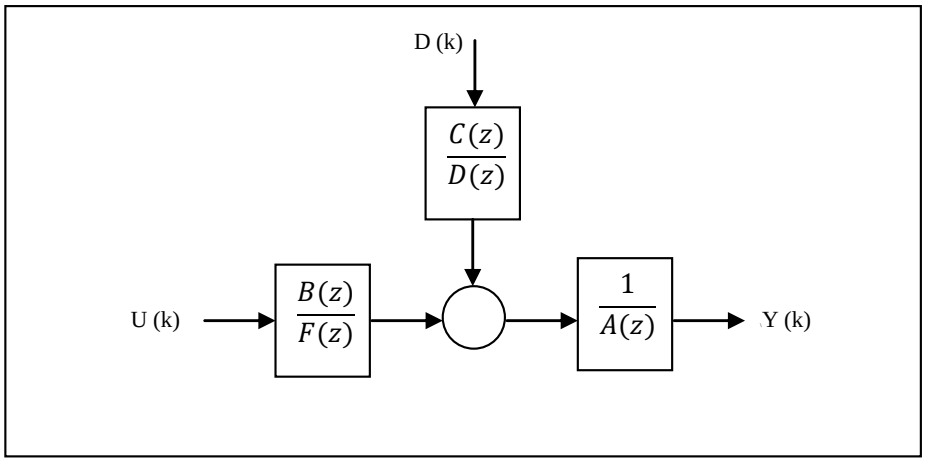

Figure 4. 1: GLP model structure

$$Y(k)=\frac{z^{-d}B(z)}{A(z)F(z)}U(k)+\frac{C(z)}{A(z)D(z)}D(k) \tag{4.1}$$

Where, A(z), B(z), C(z), D(z), F(z) are polynomials that describe the system dynamics. Y(k), U(k), and D(k) are the system response, the stimulus control input, and the disturbance input at instant time step k, respectively. Integer d is the number of the time steps delay between the stimulus control signal and the system response.

Table 4. 1: Parametric model estimation methods

Model	Inputs	Model Nature	Equation
AR Model	Error only	Stochastic	$Y(k)=\frac{1}{A(z)}D(k)$
ARX Model	Error and Exogenous	Stochastic and Deterministic	$Y(k)=\frac{z^{-d}B(z)}{A(z)}U(k)+\frac{1}{A(z)}D(k)$
ARMA Model	Error only	Stochastic only	$Y(k)=\frac{C(z)}{A(z)}D(k)$
ARMAX Model	Error and Exogenous	Stochastic and Deterministic	$Y(k)=\frac{z^{-d}B(z)}{A(z)}U(k)+\frac{C(z)}{A(z)}D(k)$
Output-Error Model	Error and Exogenous	Stochastic and Deterministic	$Y(k)=\frac{z^{-d}B(z)}{F(z)}U(k)+D(k)$
Box Jenkins Model	Error and Exogenous	Stochastic and Deterministic	$Y(k)=\frac{z^{-d}B(z)}{F(z)}U(k)+\frac{C(z)}{D(z)}D(k)$

The four basic steps for developing a dynamic model using the systems identification parametric estimation modeling methods are the following:

1- Stimulate the system and collect the needed signals (reference signal, stimulus control signal, and the output signal)

2- Select the model structure

3- Select the model polynomials' orders and estimate its parameters

4- Model validation

4.3.3 System Identification Input Signal Selection

Many predetermined input signal types can be used to stimulate the system to acquire the needed signals for the system identification modeling process. These signals are used as a reference signal R(k), in the case of closed loop system identification methods, or a stimulus control signal U(k), in the case of open loop system identification methods. The input signals can be summarized below [24][25]:

1- Instantaneous Excitation Signals

The impulse and step input signals are examples of instantaneous excitation signals. These signals have frequency bandwidth ranging from zero to infinity. Therefore, they excite the systems dynamic at all possible frequencies to identify all the system dynamics frequencies.

2- Periodic Excitation Signals

Sine, Square, Saw, and Chirp Sine are commonly used periodic excitation signals. These signals are usually preferred as input signals for the systems frequency response function analysis.

3- Random Excitation Signals

Pseudo-Random Binary Sequence (PRBS), Random Binary Signal, and Gaussian White Noise are the most common random input excitation signals. The PRBS signal is preferred to use for stochastic systems, because it contains both the periodic and the random sequence properties.

4.3.4 Open Loop vs Closed Loop System Identification

As a first alternative, open loop system identification preferred method to develop a dynamic model of the system dynamics based on the stimulus signal U(k) and the output signal Y(k), without the presence of the feedback loop. The open loop system identification is difficult to implement sometimes, because many systems cannot be operated without the presence of the feedback loop (safety issues or systems structure issues). Therefore, closed loop system identification methods can be used to determine the plant (open loop system) transfer function under the feedback loop operating conditions. Three different methods are utilized to develop a dynamic model under closed loop operating conditions [24]:

1- Direct Method

The closed loop system is stimulated with reference input signal R(k). The stimulus signal U(k) and the system response Y(k) are used to determine the open loop system dynamic model, ignoring the effect of the feedback loop on the system dynamics.

2- Indirect Method

The closed loop system is stimulated with reference input signal R(k). The reference signal R(k) and the response signal Y(k) are used to determine the closed loop system dynamic model. Then, based on the controller and previously known feedback dynamic models, the open loop system dynamic model is determined.

3- Joint Input-Output Method

The system stimulus signal U(k) and response signal Y(k) are considered as outputs of a cascaded system. The reference signal R(K) and the disturbance D(k) together excite the system, and the plant model is identified from this joint input-output system relationship.

4.4 Micro USM Cutting Force Dynamic Model Development

Developing a dynamic model of the micro USM cutting force was required to design and tune the control system off-line before implementation to prevent any unexpected system behavior. Studies show that the dynamics of the USM process is complex and hard to model analytically [26][27]. In such cases, experimental methods (system identification approach) can be used to predict the system dynamics by stimulating the system using a predetermined testing signal and observing the system response. Figure 4.2 shows the block diagram of the micro USM system under the feedback cutting force loop. Although, the micro USM system contains some sort of nonlinearity; the micro USM system under the cutting force control loop can be considered as a linear system as shown in Figure 4.3.

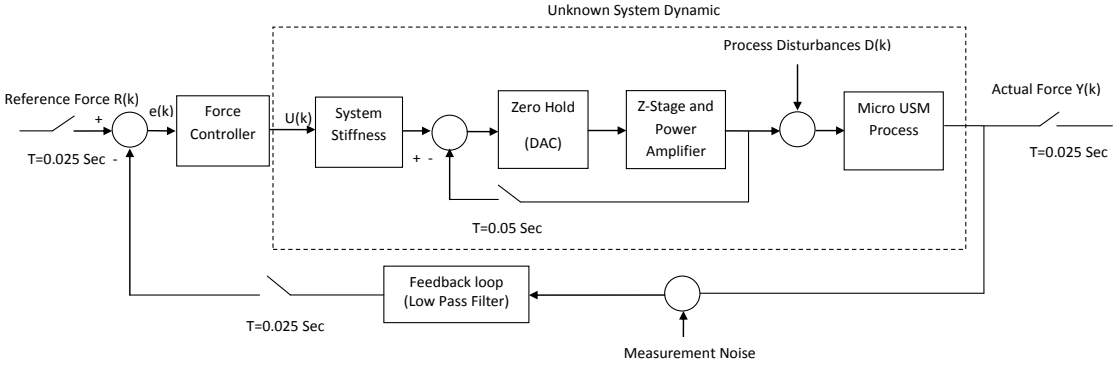

Figure 4. 2: Micro USM system block diagram under cutting force feedback loop

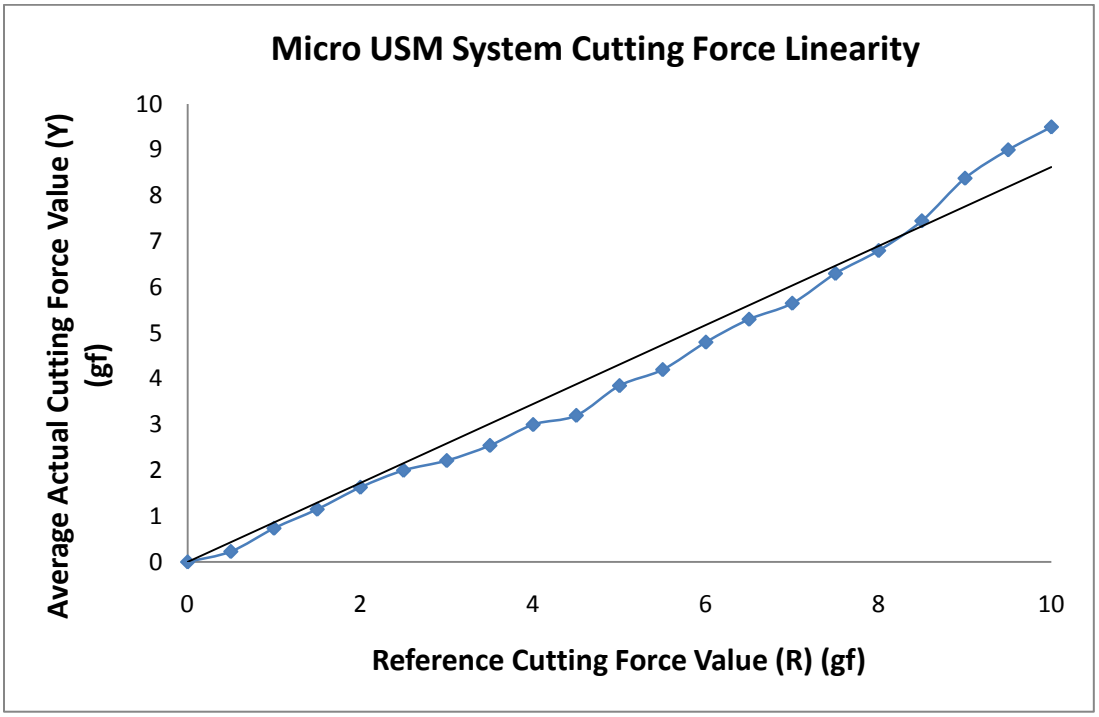

Figure 4. 3: Micro USM system cutting force linearity

First, an attempt was made to identify the system dynamics without the feedback loop (open loop system identification for the unknown system dynamics block in Figure. 4.2).The cutting force response for a step input stimulus control signal U(k) was exponentially decayed to zero without using the cutting force feedback control loop. When the system was stimulated with a step response, the Z-axis moved the tool downward to the workpiece with corresponding initial displacement, based on the system stiffness. During machining, thin layers from both the tool and the workpiece were continuously removed. After sometime, depending on the machining rate and the tool wear rate, the removed layers thickness became equal to the initial displacement and the cutting force dropped to zero. Because of the cutting force dropping, along with other

reasons such as the machine safety and tool breakage, closed loop system identification was essential to identify the micro USM system dynamics. Using the direct method closed loop system identification, an experimental based model of the micro USM cutting force dynamics was developed by stimulating the system with a test reference signal R(k) and observing the input stimulus U(k) and the actual output Y(k) with presence of the feedback loop.

In general, the dynamic behavior of the USM process varied with time depending on the machining gap conditions such as the abrasive particles shape and size, workpiece and tool material structures and properties, ultrasonic vibration amplitude and frequency, external vibrations, and environmental conditions. Therefore, the dynamic model should account for the deterministic and the stochastic nature of the process along with the process time variation behavior. An Autoregressive Moving Average Model with Exogenous Input (ARMAX) is an appropriate linear model that accounts for model deterministic and stochastic inputs dynamics and the system natural response. The ARMAX model was used to model the machining systems dynamics under such conditions [28]. The ARMAX (n,m,w,d) model at any instant k is given in Equation (4.2):

$$Y(k)+a_1Y(k-1)+a_2Y(k-2)+\ldots+a_nY(k-n)=b_0U(k-d)+b_1U(k-d-1)+\ldots+ b_mU(k-d-m)+D(k)+c_1D(k-1)+\ldots+c_wD(k-w);k=1,2,3\ldots,D(k)\sim NID(0,\sigma_a^2) \quad (4.2)$$

Where, Y(k), U(k), and D(k) are the actual cutting force, the stimulus cutting force control signal, and the disturbances of unmodeled factors of the cutting force at instant time step k, respectively. Integers n, m, and w are the order of the model polynomials that describe the system dynamics. The coefficients ($\{a_1, a_2, \ldots, a_n\}$, $\{b_0, b_1, \ldots, b_m\}$, $\{c_1, c_2, \ldots$

,c_w}) are unknown and time varying coefficients that describe the effect of the system natural response, deterministic stimulus control input, and random disturbance input, respectively, on the cutting force dynamics. Integer d describes the system time delay for the stimulus input U(k). By taking the Z-transform of both sides of the difference equation given in Equation (4.2), the discrete system transfer function of the micro USM is obtained as given in Equations (4.3.1) and Equation (4.3.2). The transfer function describes the system behavior for both the deterministic control input U(k) and the stochastic disturbance input D(k).

$$A(z)Y(k) = z^{-d}B(z)U(k) + C(z)D(k) \tag{4.3.1}$$

$$Y(k) = \frac{z^{-d}B(z)}{A(z)}U(k) + \frac{C(z)}{A(z)}D(k) \tag{4.3.2}$$

Where

$$A(z) = 1 + a_1 z^{-1} + a_2 z^{-2} + \ldots + a_n z^{-n}$$

$$B(z) = b_0 + b_1 z^{-1} + b_2 z^{-2} + \ldots + b_m z^{-m}$$

$$C(z) = 1 + c_1 z^{-1} + c_2 z^{-2} + \ldots + c_w z^{-w}$$

A(z), B(z), and C(z) are polynomials that describe the discrete transfer function dynamics of the system. Based on an extensive number of experiments, the system response for impulse and step reference inputs were found to have one time step delay (d = 1) between the input signal command and the cutting force response.

The micro USM system was excited by a PRBS signal with 5 gf cutting force amplitude and 0.025 second sequence period (equivalent to the system servo frequency)

as a reference signal R(k) using the P controller and feedback loop (when K_p = 1, the cutting force was found to be unstable under the PRBS input, therefore, K_p = 0.375 was used instead). Figure 4.4 shows the PRBS input reference signal and the actual micro USM system cutting force response under the PRBS signal. The stimulus signal U(k) and the actual cutting force signal Y(k) were recorded during machining and used as input and output signals, respectively, for direct closed loop system identification analysis.

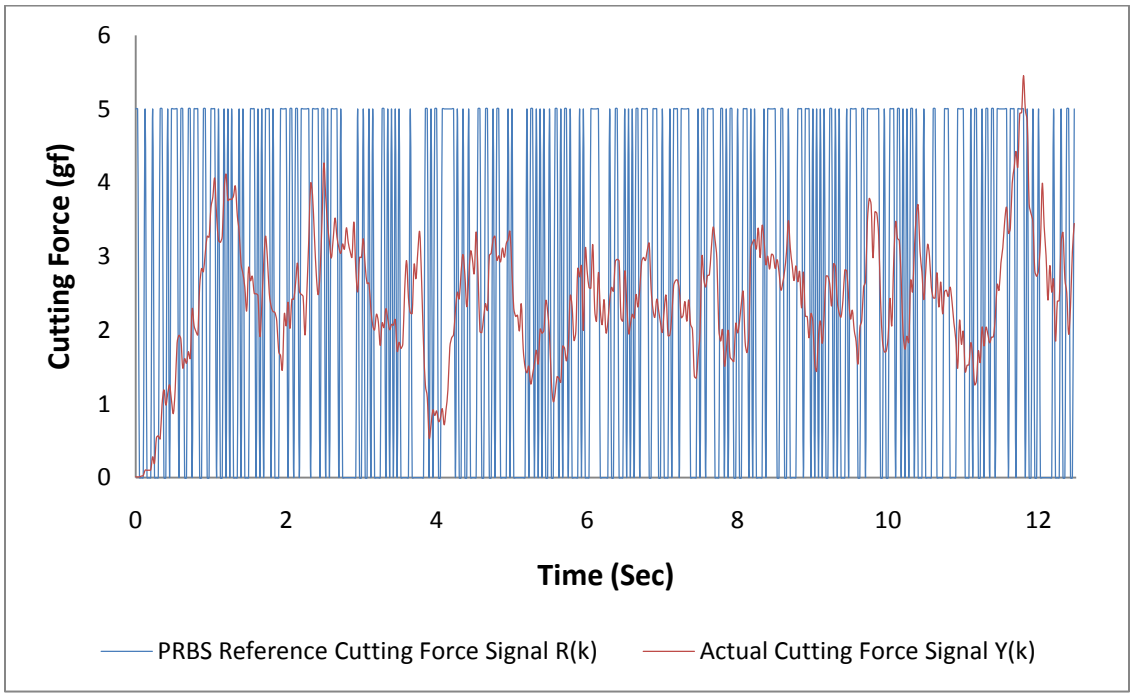

Figure 4. 4: PRBS input reference signal and the actual cutting force response for micro USM system

Analytically, the adequate system model order was found to be a higher order system. However, simplified second order system (n = 2) was found to be appropriate to describe the system dynamics behavior for many machining processes [28] [29] and also for the micro USM system. Table 4.2 shows that ARMAX(2,1,1,1) was found to be a

statistically adequate model to describe the micro USM system dynamics (the F-test value was more than the critical value [$F_{0.95}(6, , \infty) = 2.1$] just when n = 2). The orders of transfer function numerators (m, and w) have to be less than the transfer function denominator order (n). Therefore, ARMAX(2,1,1,1) was used to predict the system dynamics behavior for micro USM system. The polynomials' coefficients of the ARMAX(2,1,1,1) model were estimated to minimize the square error between the model and the actual cutting force. Then the model was used to predict the cutting force value based on the current and previous values of the stimulus control input U(k) and the disturbance input D(k) signals values (See appendix A for the Simulink [The MathWorks, Inc., MI] computer simulation model of the cutting force based on the ARMAX model). Figure 4.5 shows the actual cutting force Y(k) under the PRBS signal as a reference cutting force signal R(k) and of the cutting force prediction using the ARMAX(2,1,1,1) model.

Table 4. 2: ARMAX model order selection

Model	**MSE**	**RSS**	**F-Test**
ARMAX(2,1,1,1)	0.11593	57.965	18.4269
ARMAX(4,3,3,1)	0.11367	56.835	0.03582
ARMAX(6,5,5,1)	0.11056	55.280	0.04325

SS Total = 344.2564, Number of data points (N) = 500, $F_{0.95}(6, \infty) = 2.1$

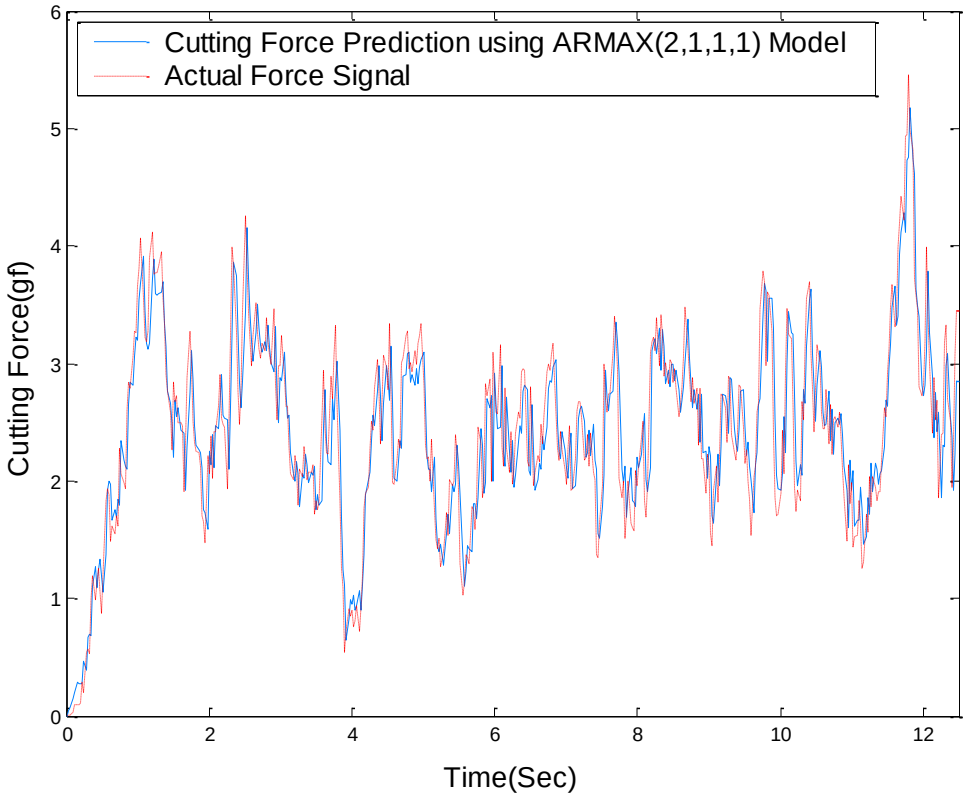

Figure 4. 5: Actual cutting force vs cutting force prediction using the ARMAX(2,1,1,1) model [a_1 = -1.85007, a_2 = 0.85014, b_0 = 0.0068588, b_1 = 0, c_1 = -0.9862, d = 1, T = 0.025 sec, = 0.1159 gf^2] for a PRBS input as a reference signal

4.5 Model Validation

For validation purposes, the ARMAX (2,1,1,1) model was then used to predict the cutting force response for a step input (K_p = 0.1, 5 gf) as a reference signal R(k). The ARMAX(2,1,1,1) model prediction for cutting force response under a step input follows the actual cutting force signal acquired using the same machining conditions (step response, K_p = 0.1, 5 gf) as shown in Figure 4.6. In addition, Figure 4.6 shows the advantage of using both the stochastic and the deterministic parts of the ARMAX model compare to the deterministic part only to predict the micro USM cutting force dynamics.

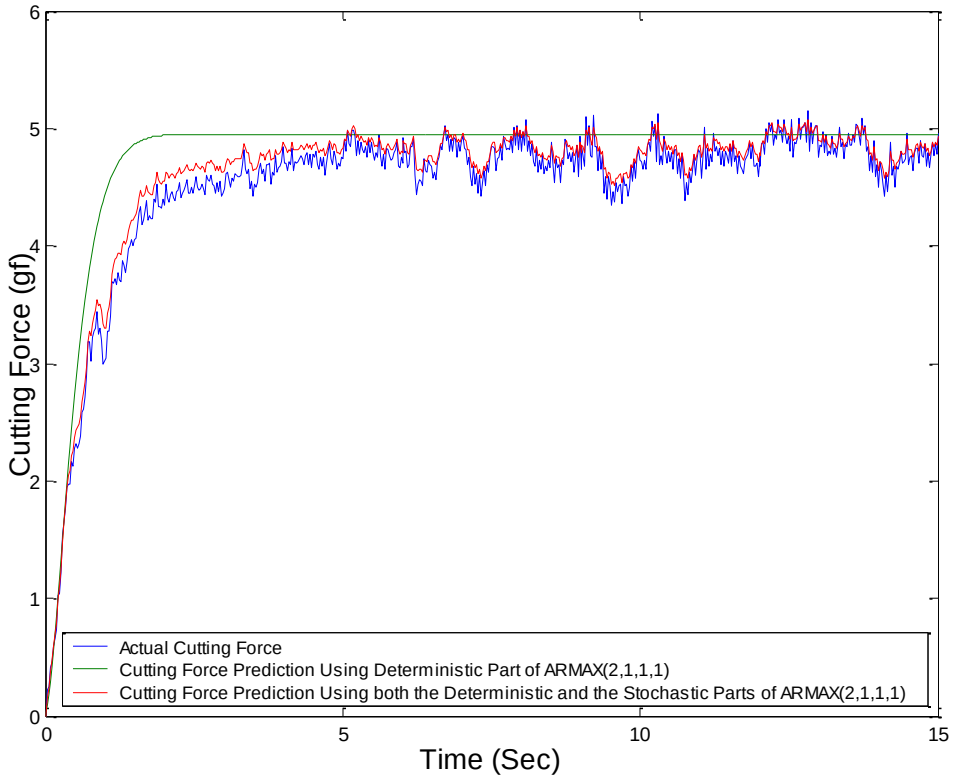

Figure 4. 6: Actual cutting force vs cutting force prediction using the ARMAX (2,1,1,1) for step input [a_1 = -1.85007, a_2 = 0.85014, b_0 = 0.0068588, b_1 = 0, c_1 = -0.9862, d = 1, T = 0.025 sec] model for a step input (K_p = 0.1, 5 gf)

CHAPTER 5

CONTROL SYSTEM DESIGN AND IMPLEMENTATION

5.1 Introduction

Uncontrolled micro USM cutting force was observed to influence the machining performance and the material removal mechanism stability. In Chapter 3, the micro USM system has been modified to facilitate the implementation of different cutting force controller structures. A dynamic model of the micro USM cutting force is also developed in Chapter 4. In this chapter, different controller structures are designed and implemented to stabilize the micro USM cutting force. Moreover, the effects of these cutting force controllers on the micro USM process stability and machining characteristics are analyzed.

5.2 Cutting Force Control

In machining processes where the material is removed by mechanical action such as milling [30], grinding [31], and turning [32], controlling the cutting force was found to improve the process stability. Different adaptive control mechanisms showed advantages in stabilizing the cutting force for different machining processes under time varied conditions [33] [34]. For micromachining, stabilizing the cutting force was found to be essential to prevent the micro tool breakage and enhance the machining productivity for micro holes drilling [35]. Because the cutting force in micro USM is very small, the cutting force variations were found to have a significant effect on the machining characteristics [3]. Moreover, the cutting force variations and overshoot could cause tool

breakage and surface damage at the micro level. Therefore, controlling the micro USM cutting force is required to improve the process stability.

In the micro USM, abrasive particles present between the micro tool and the ultrasonically vibrated workpiece cause the material to chip away from both the workpiece and the tool. During machining, the tool is fed downwards to compensate for the removed layers from both the workpiece and the tool. The tool feed occurs under either a constant feed rate or a constant cutting force, usually known as constant static force. In the micro USM, constant cutting force mode control is widely implemented to prevent tool breakage and to precisely control the removed unit volume. Micro USM process cutting force control is difficult to accomplish, because the required cutting force value is low, in range of several grams, and the cutting process is highly stochastic depending on the size and shape of the abrasive particles engaged instantly in the cutting process. To stabilize the micro USM process, AE signal was also utilized as a feedback signal instead of the cutting force signal [14]. However, the AE signal has no physical meaning as a process parameter like the cutting force. The AE signal was also found to have different signal levels at different workpiece positions and machining times [14]. Therefore, using the cutting force signal as a feedback signal to stabilize the micro USM process was more convenient.

5.3 Cutting Force Control Objectives for Micro USM

The main objective of the cutting force control is to maintain constant cutting force during machining. The cutting force varies with time, because the cutting load transmits into the workpiece through abrasive particles of random size and shape. Moreover, the

ultrasonic vibration is a high frequency vibration, and it is difficult to observe its effects on the cutting force using the load cell sensor. The effects of the abrasive particles, high frequency ultrasonic vibration, and the sensor measurement noise along with many other factors related to the machining conditions and the machining environment are neglected. The effects of these factors come into play as random disturbances. The disturbances from these factors have some low frequency dynamics that can be extracted to make the disturbance input D(k) look like a white noise. Therefore, it is impossible to have a cutting force signal with zero cutting force variations. However, minimizing the cutting force variations is necessary to stabilize the micro USM process.

The Steady State Error (SSE) of the cutting force should also be zero to ensure that the system follows the desired cutting force. Even though the effect of the transient response appears clearly just at the beginning of machining, sped up transient response is required to minimize the cutting force variations. For example, when the machining takes place in the machining gap, the tool must be fed downwards to compensate for the removed layers from both the tool and the workpiece; each control cycle the tool moves downward and has an effect like an impulse cutting force input on the micro USM system. The convolutions of these impulse responses with time add more variations to the cutting force signal. Finally, the overshoot in the cutting force leads to tool breakage and deep indentations and cracks on the machined surface, especially at the finishing stage. Therefore, the objectives of the cutting force control are to:

1- minimize the cutting force variations

2- eliminate the steady state error

3- improve the system disturbance rejection

4- speed up the system transient response

5- eliminate the cutting force overshoot

By achieving these objectives, the machining performance of micro USM process is expected to improve. However, minimizing cutting force variations and eliminating the steady state error are the two primarily control objectives that should be achieved.

5.4 Cutting Force Control System Design and Implementation

To achieve the micro USM cutting force control objectives, different computer controller structures were designed and implemented. These controllers were optimized off-line using a computer simulation model based on the ARMAX cutting force model.

5.4.1 Proportional (P) and Proportional-Integral (PI) Controllers

As the first alternative, The P controller was implemented to stabilize the cutting force. Through a large number of experiments, the cutting force of micro USM under the P controller (using the same controller structure illustrated in Figure 4.2) was found to have high cutting force variations (ranging from 0 up to 18 gf for 5 gf cutting force set point) and large steady state errors (up to 0.45 gf for 5 gf cutting force set point), even under optimized proportional gain value. The cutting force signal was also found to have large cutting force overshoot under high proportional gain values. Initially, an attempt was made to design a Proportional–Integral–Derivative (PID) controller instead of the P controller. The control signal component from the derivative term of the PID controller was found to be very high compared to these from the proportional and the integral terms because of the cutting force high frequency measurements noise. The micro USM cutting

force was unstable under the PID controller. Therefore, a PI controller was used to stabilize the cutting force instead of the PID controller.

The transfer function of micro USM cutting force was used to simulate the system behavior under different proportional gain (K_p) and integral time (T_i). The discrete PI controller algorithm using trapezoidal integration method was utilized as given in Equation (5.1) [36].

$$U(k) = K_p\left[e(k) + \frac{1}{T_i}\sum_{i=1}^{k}\left(\frac{e(i)+e(i-1)}{2}\right)T \right] \tag{5.1}$$

Where, U(k) and e(k) are the controller output and the error signal at instant k, respectively. K_p is the proportional gain and T_i is the integral time in minutes. T is the servo control time step period.

Computer simulations of the P and the PI controllers based on the discrete system transfer function were used to tune the controller parameters off-line to achieve the control objectives (using the Simulink (The MathWorks, Inc., MI) model in appendix B). On-line fine tuning for both the P and the PI controllers was performed. The best cutting force control was obtained with $K_p = 0.5$ for the P controller and $K_p = 0.5$ and $T_i = 0.4$ for the PI controller. Figure 5.1 and Figure 5.3 show the cutting force response signals recorded during machining of three different holes using the P and the PI controllers, respectively. Moreover, Figure 5.2 and Figure 5.4 show the SEM images of the machined holes using the P and the PI controllers, respectively.

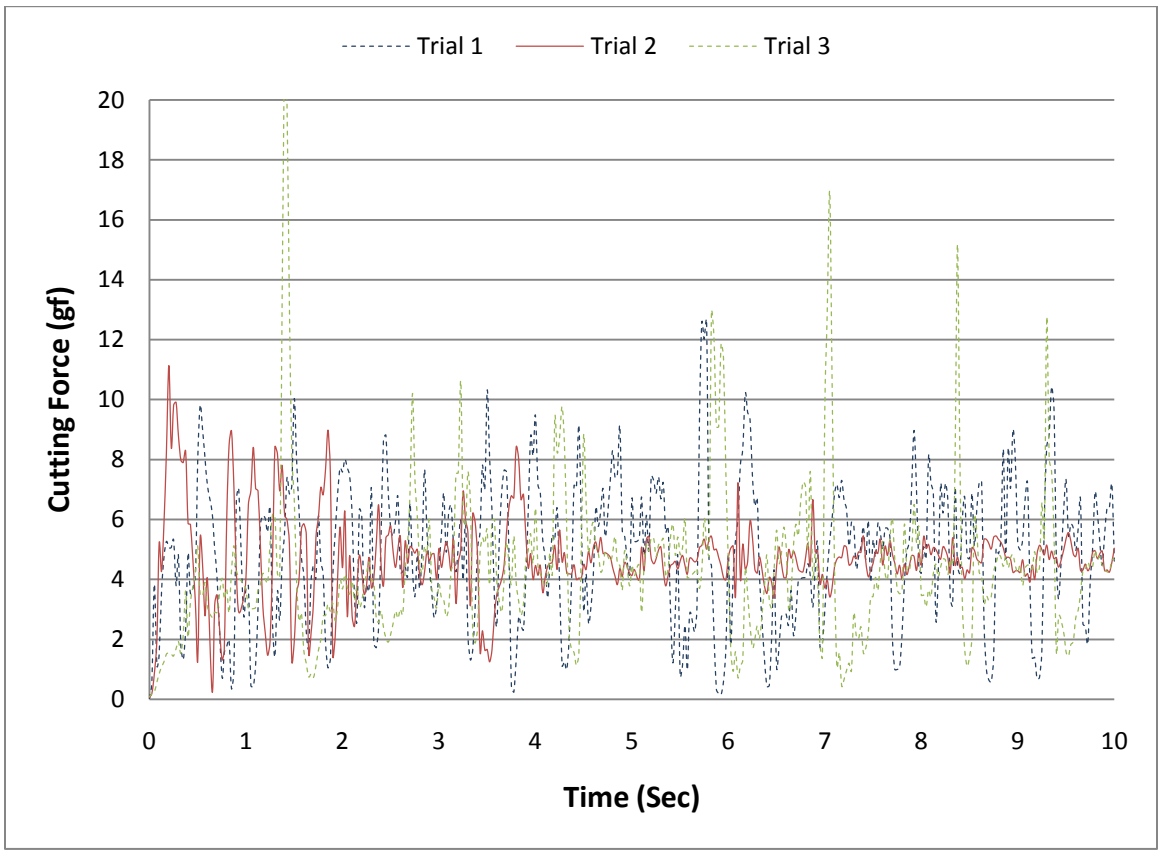

Figure 5. 1: P controller cutting force responses for three different holes (K_p = 0.5, 5 gf)

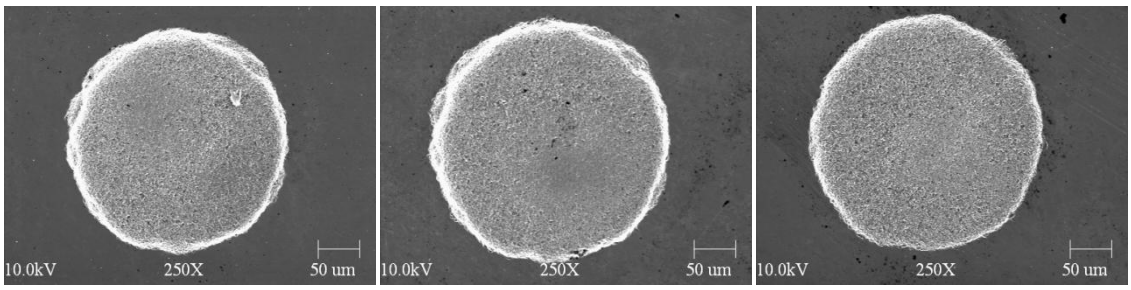

Figure 5. 2: SEM images for the three different holes machined using the P controller (Trail 1, 2, and 3 respectively)

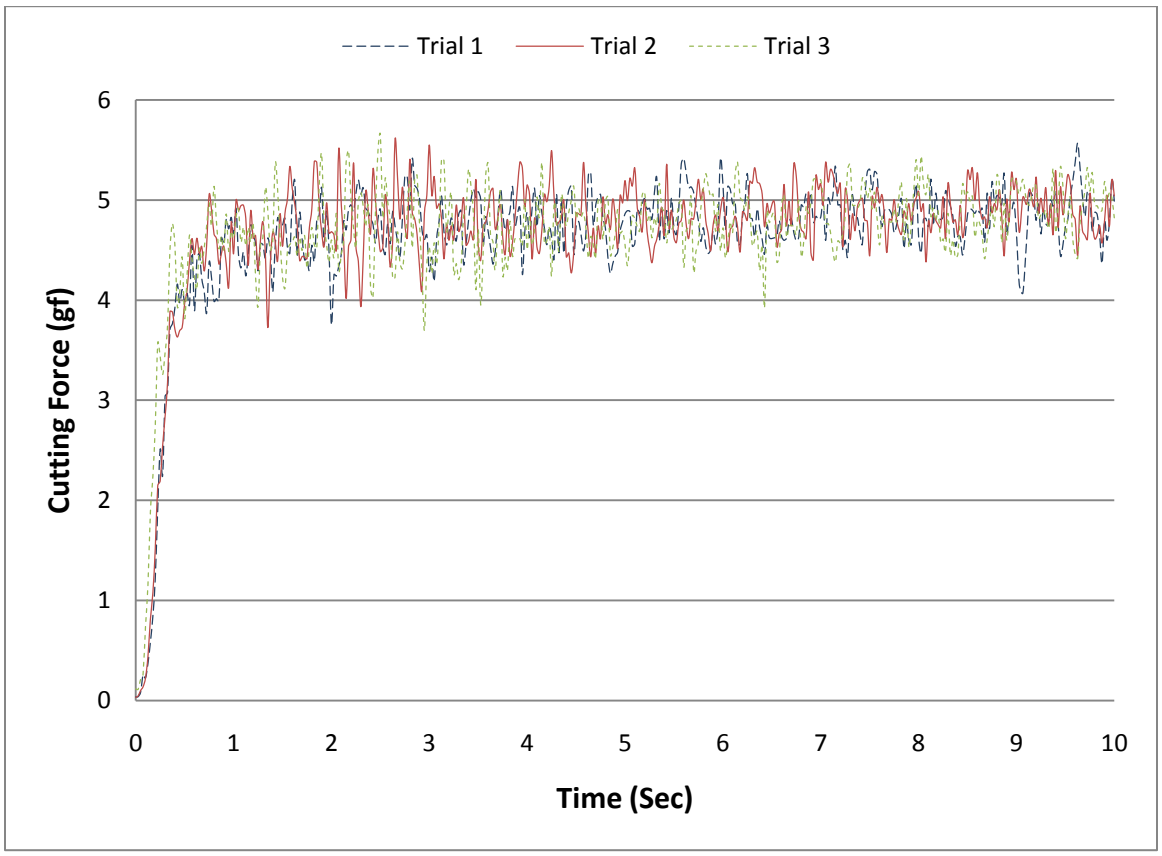

Figure 5. 3: PI controller cutting force responses for three different holes (K_p = 0.5, T_i = 0.4, 5 gf)

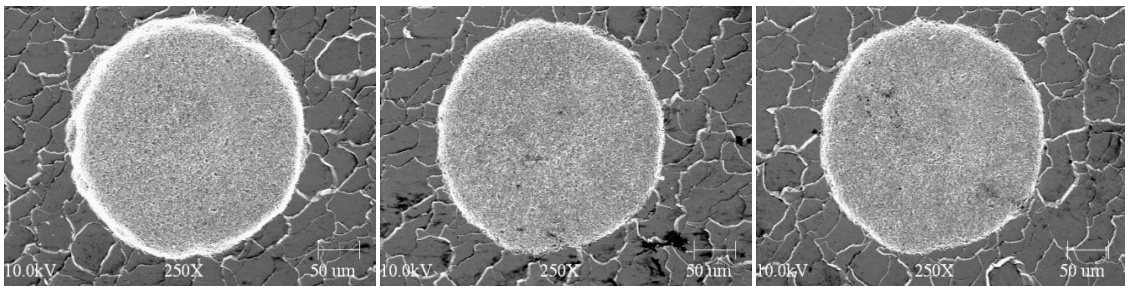

Figure 5. 4: SEM images for the three different holes machined using the PI controller (Trail 1, 2, and 3 respectively)

5.4.2 Model Reference Adaptive Control (MRAC)

The PI controller showed an improvement over the P controller by reducing the cutting force variations. However, the performance of the PI controller was observed to be highly sensitive to the machining conditions and the controller's gains. The PI controller also needs to be tuned for all possible machining conditions before implementation. Therefore, an adaptive control mechanism is needed to account for the system dynamics time varied behavior under different machining conditions. Because it is simple and easy to implement, the MRAC controller is a commonly used adaptive control strategy. The MRAC controller was utilized to stabilize different machining processes such as turning [32], milling [37], and EDM [38]. Many MRAC structures were designed and implemented, but the simple feedforward MRAC controller was found to satisfy the micro USM cutting force control objectives. Figure 5.5 shows the structure of the feedforward MRAC controller that was used to control the cutting force in the micro USM. The cost function J(t) was selected to minimize the square error $e_m(t)^2$ between the plant response $y_p(t)$ and the reference model response $y_m(t)$ forcing the system G_p to behave similar to the reference model G_m. Equations (5.2 - 5.5) describe the adaptation laws for the Feedforwad Gain (K_{ff}) for feedforwad MRAC controller using MIT rule [39]. The final discrete difference equation of the adaptation mechanism gain K_{ff} is given in Equation (5.6).

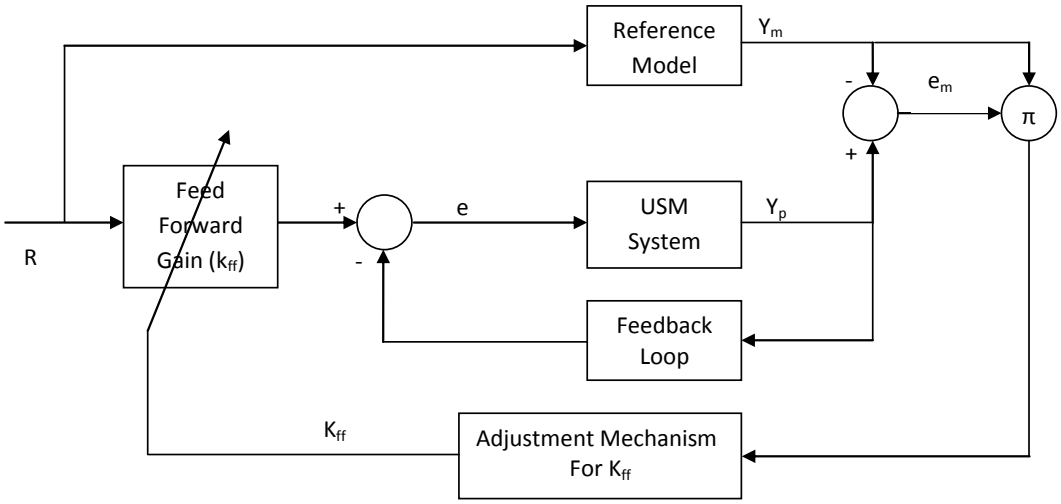

Figure 5. 5: Feedforward MRAC structure for micro USM system

$$J(t) = \frac{1}{2} e_m(t)^2 \tag{5.2}$$

$$e_m(t) = Y_p(t) - Y_m(t) \tag{5.3}$$

$$\frac{dK_{ff}}{dt} = -\gamma\, e_m(t) \frac{de_m(t)}{dK_{ff}} \tag{5.4}$$

$$\frac{dK_{ff}}{dt} = -\gamma\, e_m(t) Y_m(t) \tag{5.5}$$

$$K_{ff}(k) = K_{ff}(k-1) - \gamma\, e_m(k-1) Y_m(k-1) \tag{5.6}$$

Where, Gamma (γ) is the adaptation coefficient selected based on the process dynamics. The reference model G_m was selected to be as a second order model with SSE = 0, Settling Time (T_s) = 1 second, and Damping Ratio (ζ) = 0.707. First, the deterministic part of the ARMAX model (using the Simulink (The MathWorks, Inc., MI) model in appendix C) was used to tune the γ value off-line under two unit impulse

disturbance inputs (at time t = 15 seconds and t = 25 seconds) as shown in Figure 5.6. The adaptation coefficient (γ) value was tuned on-line and found to be around the simulated gamma value γ = 0.001 from the simulation optimization analysis. The MRAC algorithm was implemented and three holes are machined under the same machining conditions that are used for the P and the PI controllers. The results of the cutting force signal response under the MRAC controller and the cutting force signals are shown in Figure 5.7. The SEM images of the machined holes using the MRAC controller are shown in Figure 5.8.

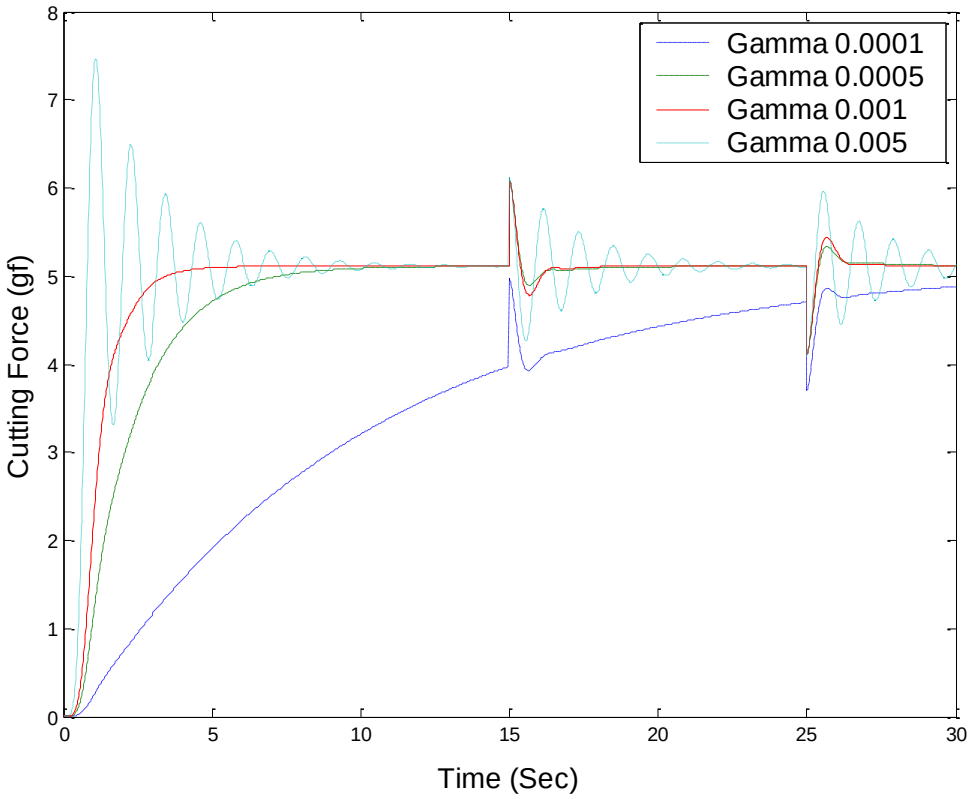

Figure 5. 6: Simulation of MRAC controller behavior for different γ value based on ARMAX model of micro USM

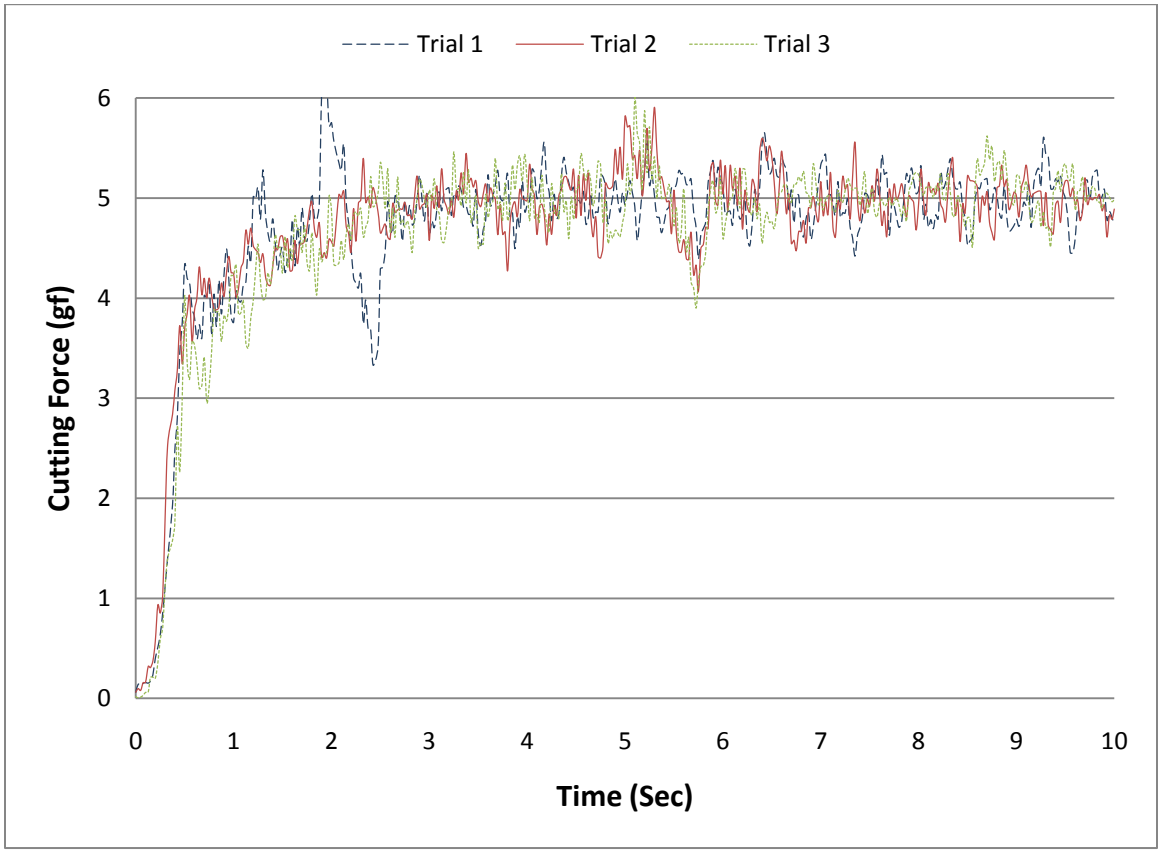

Figure 5. 7: MRAC controller cutting force responses for three different holes (γ = 0.001, 5 gf)

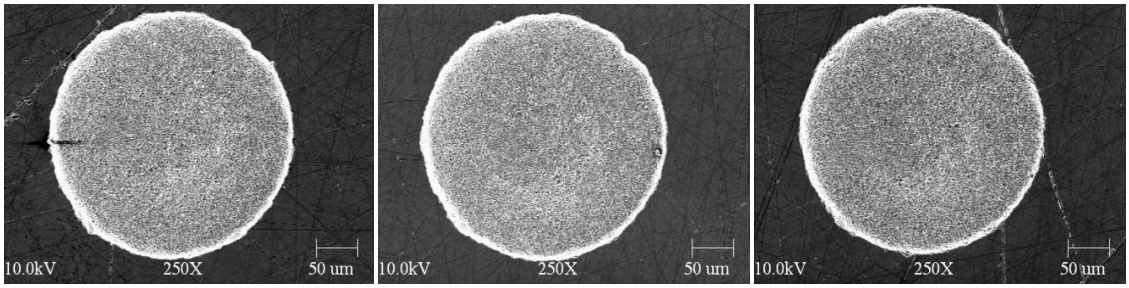

Figure 5. 8: SEM images for the three different holes machined using the MRAC controller (Trail 1, 2, and 3 respectively)

5.5 Micro USM Process Stability Analysis

5.5.1 Cutting Force Control

The statistics of the actual cutting force signal for steady state response (time > 2 seconds) for the P, PI, and MRAC controllers are summarized in Table 5.1. In general, both the PI and the MRAC controllers showed better cutting force control over the P controller. The SSE, difference between the signal average and the desired value, values were unrepeatable under the P controller (ranging from 0.01 to 0.45 gf). Even though the PI controller should reduce the cutting force SSE, the SSE value of the micro USM cutting force under the PI controller were high (ranging from 0.15 to 0.19 gf), because it was difficult to keep the cutting force variations low using a small integration time period (T_i). Using larger integration time period (T_i) values limited the ability of the PI controller to eliminate the cutting force SSE. The SSE values were found to be the smallest for the MRAC controller ($|SSE| < 0.05$ gf).

Both PI and MRAC controllers reduced the cutting force variations compared to the P controller (at least by 66%). The difference between the cutting force signal Standard Deviation (S.D.) for the PI and the MRAC controllers was found to be insignificant compared to the cutting force set point. Therefore, both the PI and the MRAC controllers were considered to have the same effect on reducing the cutting force variations. Based on both the cutting force variations and the SSE criteria, the MRAC controller was the best cutting force for the micro USM system (compared to the P and PI controllers). The PI controller is found to be less sensitive to the cutting force measurements noise because it averages out the positive and the negative noises during the integration period.

Therefore, the ability of the PI controller was higher in improving the system disturbances rejection from both the measurements noise and the cutting process.

The effect of the cutting force variations on the material removal mechanism is clearly demonstrated for a single sharp abrasive particle as shown in Figure 5.9. High cutting force variations generate variable indentations depths for the same abrasive particle depending on the instantaneous cutting force value (combination of Case 1, Case 2, and Case 3 in Figure 5.9 occur for the same abrasive particle based on the instantaneous cutting force value). Under controlled cutting force, the indentation depths and diameters for the same particle are more consistent (Case 2 only in Figure 5.9). Therefore, the material removal mechanism is less affected by the instantaneous cutting force, but more affected by the cutting force set point signal value.

Table 5. 1: P, PI, and MRAC controllers cutting forces statistics for steady state responses (time > 2 seconds)

Controller	**P**			**PI**			**MRAC**		
Trial No	**T 1**	**T 2**	**T 3**	**T1**	**T 2**	**T 3**	**T 1**	**T 2**	**T 3**
Avg. (gf)	5.01	4.65	4.55	4.82	4.85	4.81	4.95	4.98	4.98
SSE (gf)	0.01	0.35	0.45	0.18	0.15	0.19	0.05	0.02	0.02
S. D. (gf)	2.36	1.02	2.68	0.26	0.27	0.31	0.34	0.29	0.30
Min (gf)	0.16	1.25	0.45	4.07	3.93	3.70	3.33	4.07	3.90
Max (gf)	12.64	8.42	16.94	5.56	5.60	5.65	5.65	5.91	5.60
Range (gf)	12.48	7.17	16.49	1.49	1.67	1.95	2.32	1.84	1.70

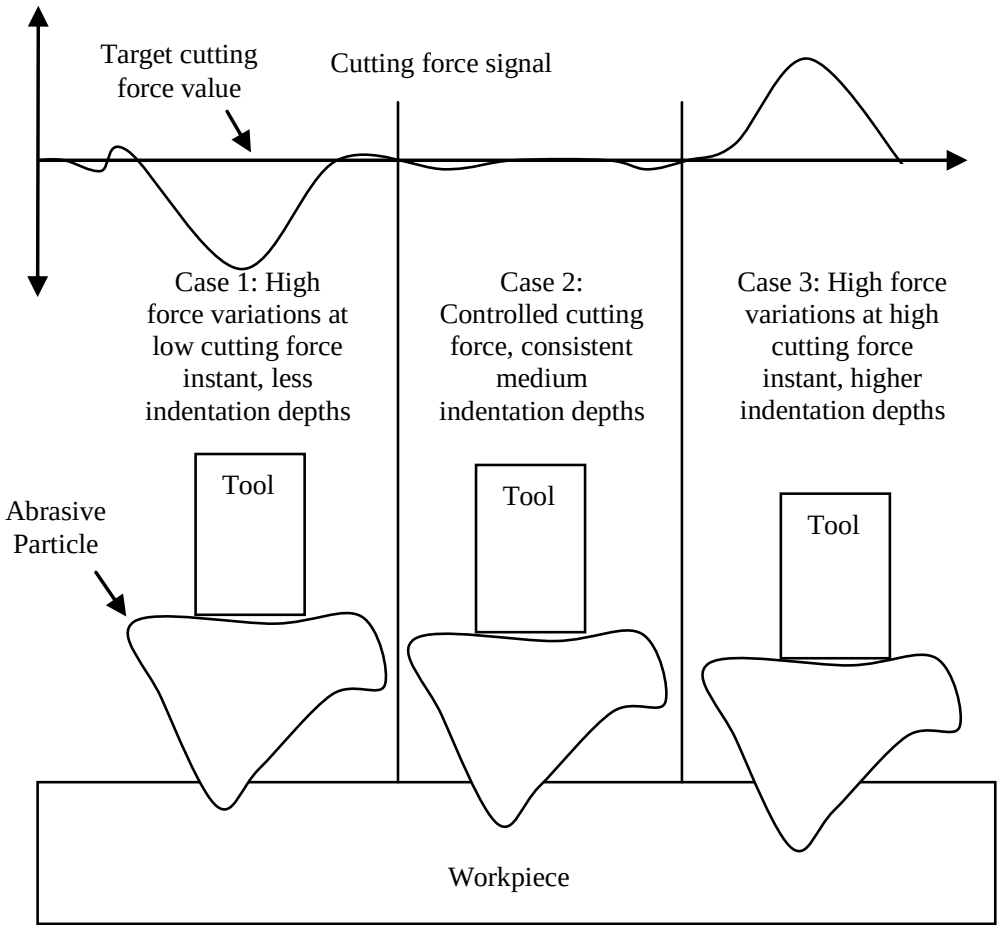

Figure 5. 9: Effect of the cutting force variations on the indentation depths for single abrasive particle

5.5.2 Effect of the Cutting Force Control on the Surface Integrities

Figure 5.10 shows the comparison of the three different control methods in terms of the surface roughness. The surface roughness generated under the P controller was higher than the PI and the MRAC controllers. The surface roughness measures produced under the P controller were highest with lowest repeatability, because the cutting force variations were higher under the P controller. The higher the cutting force variations for

the same abrasive particle, the deeper the indentation depths could be generated (Case 3 in Figure 5.9) and the rougher surfaces are produced. The PI controller produced sometimes lower and sometimes higher surface roughness compared to the MRAC controller. The MRAC controller produces the highest surface roughness repeatability. Therefore, the MRAC controller is considered to give the lowest surface roughness with the highest surface roughness repeatability.

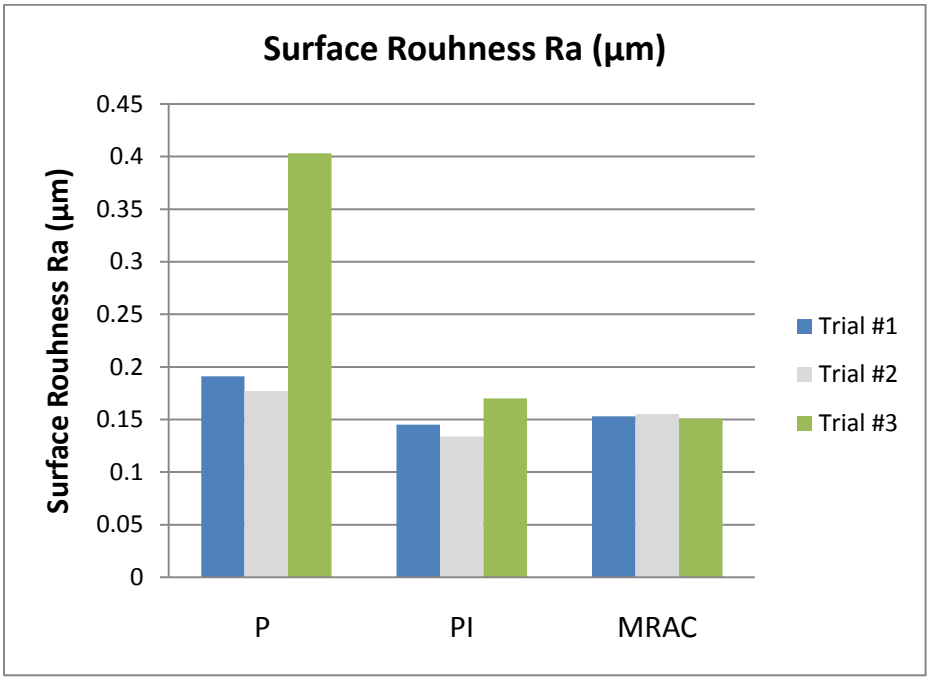

Figure 5. 10: Micro USM surface roughness measurements under different control methods

Figure 5.11, Figure 5.12, and Figure 5.13 show the SEM images of the machined surfaces using the P, PI, and MRAC controllers, respectively. The SEM pictures show that the machined surfaces under the P controller were rougher than the PI and the MRAC controllers because of the high cutting force variations. Moreover, the machined surfaces indentation diameters and depths under the MRAC controller were more consistent compared to both the P and the PI controllers.

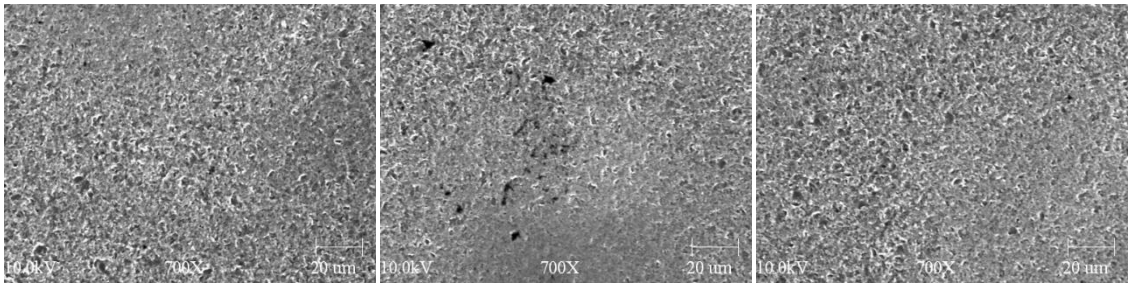

Figure 5. 11: SEM images of the machined surfaces using the P controller (Trail 1, 2, and 3 respectively)

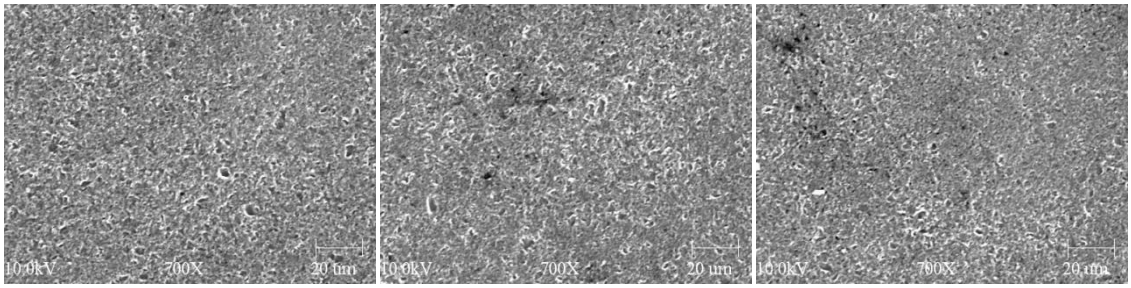

Figure 5. 12: SEM images of the machined surfaces using the PI controller (Trail 1, 2, and 3 respectively)

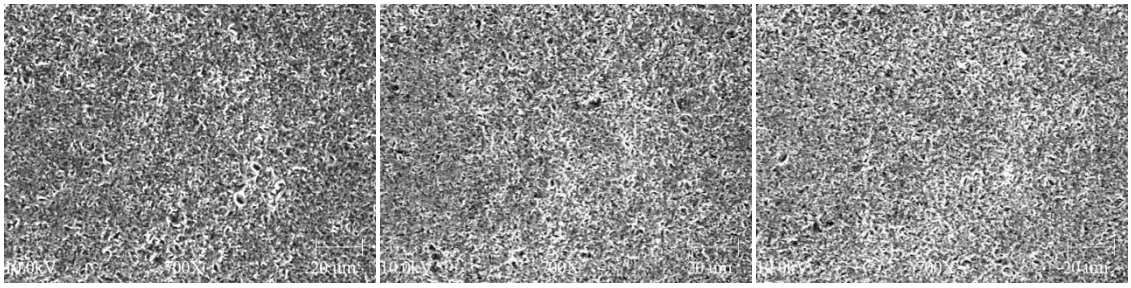

Figure 5. 13: SEM images of the machined surfaces using the MRAC controller (Trail 1, 2, and 3 respectively)

5.5.3 Effect of the Cutting Force Control on the Machining Rates

Figure 5.14 shows comparison of the three different control methods in terms of the machining rate. The machining rate under the P controller was the lowest because of the high cutting force variations. The high cutting force overshoot or cutting force variations give the controller false indication that the cutting force increases very fast; the controller reacts by moving the tool upwards to reduce the cutting force. The P controller overreacts

and moves the tool upwards farther than required to stabilize the cutting force, decreasing the effective cutting force per particle. Sometimes the tool even moves far away and the cutting force drops down to zero (no machining). The indentation depths per particle decreases while the tool is being moved upwards and downwards to stabilize the cutting force leading to a decrease in the machining rate. The effect of the cutting force variations on the machining rate is illustrated in Figure 5.15. The cutting force variations under the P controller were varied with the time; when the cutting force variations were very high, from 6 to 12 seconds, the machining rate (slope of the machining depth curve) was close to zero.

Therefore, the PI and the MRAC controllers have better machining rates compared to the P controller (high cutting force variations). The PI controller has the best machining rate because it is less sensitive to the measurements noise effect and averages out the error signal during the integration period. Therefore, the effective machining time and the indention force per particle for PI controller are higher than the MRAC and the P controllers, where the tool is moving upwards and downwards to stabilize the cutting force instantaneous error that mainly contains the measurement error. Moreover, the highest machining rates repeatability was observed under the MRAC controller.

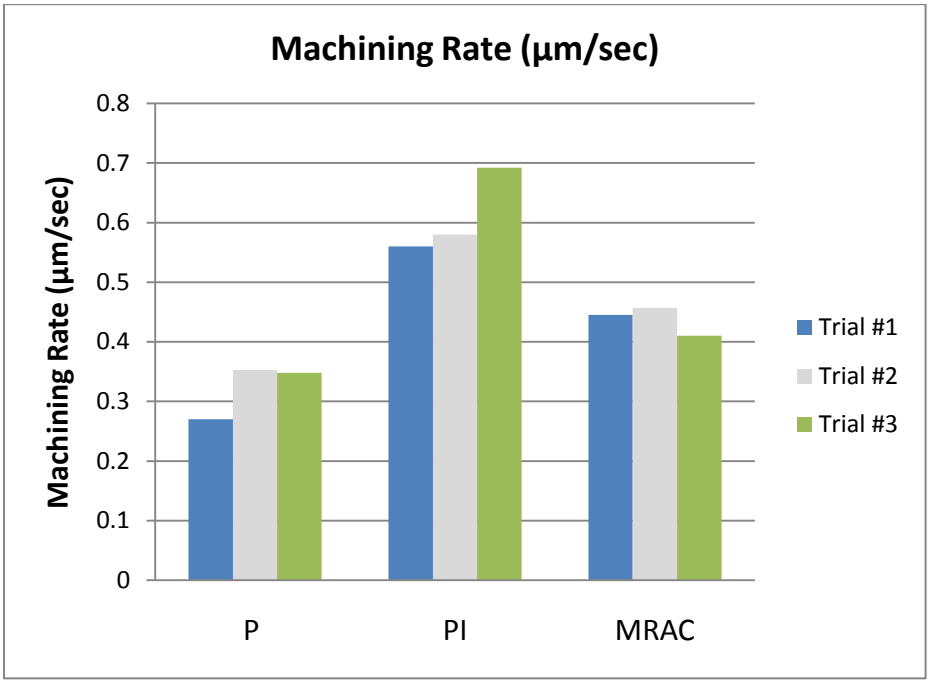

Figure 5. 14: Micro USM machining rates under different control methods

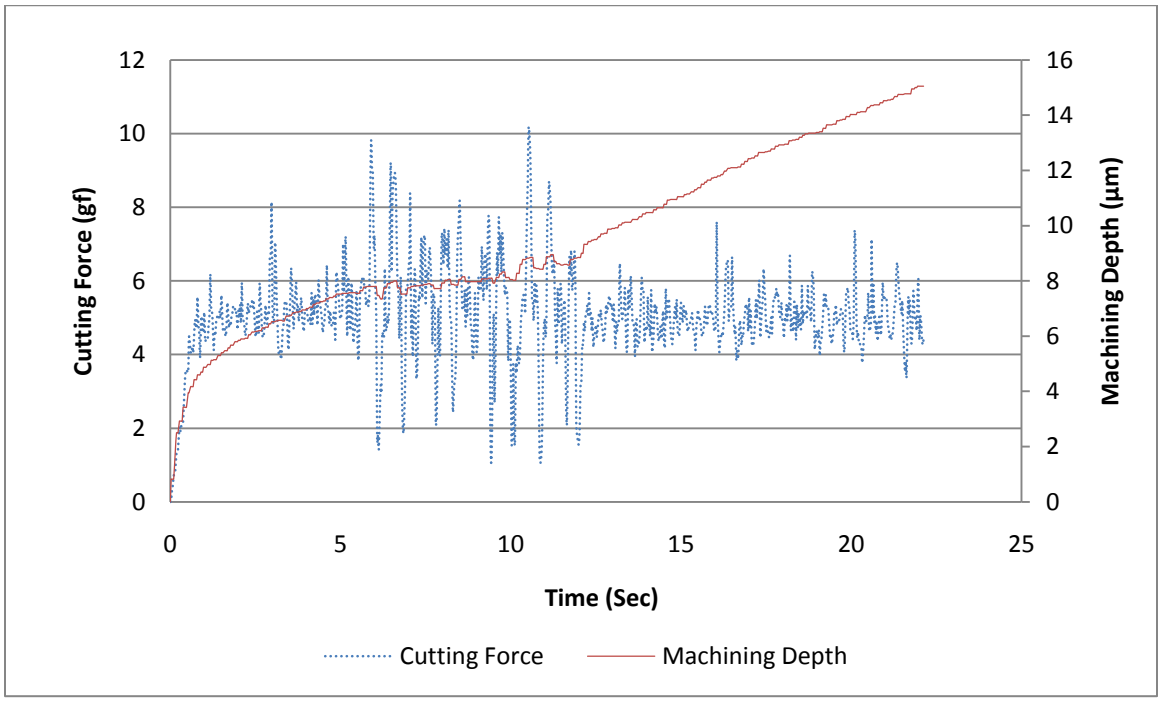

Figure 5. 15: Effect of the cutting force variations on the machining rate (P controller, K_p = 0.5, 5 gf)

CHAPTER 6

CONCLUSIONS AND RECOMMENDATIONS

6.1 Conclusions

For the micro USM system structure used, the following conclusions are drawn from this thesis work:

1- Increasing the cutting force sampling and servo control frequencies, from 5 to 40 Hz, improves the micro USM system cutting force response and eliminates the cutting force overshoot.

2- A second order ARMAX model is found to be appropriate to estimate the cutting force dynamics of the micro USM system. The second order ARMAX model predicts 83% of the cutting force variations under the PRBS testing reference input signal.

3- Three different control methods (P, PI, and MRAC) are designed and implemented to stabilize the micro USM cutting force. The MRAC and PI controllers reduce the cutting force variations at least by 66% compared to that of the P controller. Moreover, the MRAC controller gives the lowest cutting force steady state error values ($|SEE| < 1\%$). Based on both the cutting force variations and the steady state error criteria, the MRAC achieves the best cutting force control.

4- The MRAC controller shows the best performance in terms of reducing the surface roughness with increasing the repeatability of the machined holes' surfaces roughness (Ra within $\pm$ 0.05 µm).

5- The PI controller gives the highest machining rate compared to the P and MRAC controllers. However, the MRAC controller gives the highest machining rate repeatability.

6- Improving the micro USM cutting force stability is found to improve the repeatability of the micro USM machining characteristics (machining rate and surface quality).

7- The MRAC cutting force controller should be implemented on the micro USM system to eliminate the cutting force SSE, reduce the cutting force variations, and improve the repeatability of the machining rates and the machined holes' surfaces.

6.2 Recommendations for Future Work

1- Self-tuned adaptive controllers can be used to improve the process stability by incorporating a recursive ARMAX model as on-line system identification with the PI controller. Such controller structures will embed the advantages of both the PI and the MRAC controllers, with the online system identification to account for the time varied process dynamics.

2- Other controller structures such as fuzzy logic are needed to merge more than one feedback control signal like the cutting force and the AE signal to take advantage of both signals' capabilities. A sliding mode controller could also be used to account for the process nonlinearity of micro USM.

3- A better nano accuracy and repeatability Z-axis stage must be used to improve the system motion control at the micro level. Such a stage will improve the system cutting force control accuracy. It is recommended to use a stage in the range of

± 1-5 nm accuracy and repeatability (currently used stages have a theoretical resolution of ± 25 nm and repeatability of ± 25 nm).

4- The accuracy and repeatability of the currently used load cell are the best available option on the market. However, improving the load cell measurement's accuracy and repeatability are expected to improve the process stability and control. Therefore, a custom-made or a newly developed load cell sensor should be used to improve the system control accuracy in the future.

5- As discussed in Chapter 3, the tool rotation increases the cutting force variations because of the tool eccentricity and the tool holding and attaching mechanism. The NSK spindle (ASTRO-E 250, NSK America) with accuracy of ± 1 μm was utilized to improve the micro machine tool's accuracy for micromachining applications. This spindle can be utilized as a tool rotation mechanism for the micro USM to reduce the cutting force variations. This spindle set includes the driving motor, variable speed motor controller, ceramic bearing spindle, and micro tool holder (chuck). Moreover, the proposed spindle will improve the rotational speed control by overcoming the variable friction problem that led to the variable rotational speed on the currently used micro USM system.

6- It is recommended to study the effect of the cutting force variations and other dynamic factors such as the tool rotational speed, the abrasive particles size, and the vibration amplitude on the micro machined features' dimensional accuracy.

REFERENCES

[1] K. P. Rajurkar, and W. M. Wang, "Nontraditional Machining," CRC Handbook of Mechanical Engineering-Ch.13, 1997, pp. 29-34.

[2] T. C. Lee, and C. W. Chan, "Mechanism of the Ultrasonic Machining of Ceramic Composites," Journal of Materials Processing Technology, 1997, vol. 71, no. 2, pp. 195-201.

[3] X. Hu, "Mechanism, Characteristics and Modeling of Micro Ultrasonic Machining," PhD Dissertation, University of Nebraska-Lincoln, 2007.

[4] X. Hu, Z. Yu, and K. P. Rajurkar, "Experimental Study of Micro Ultrasonic Vibration Machining," In Fourteenth International Symposium on Processing and Fabrication of Advanced Materials, 2005, pp. 197-210.

[5] X. Hu, Z. Yu, and K. P. Rajurkar, "Influence of Workpiece Materials on Machining Performance in Micro Ultrasonic Machining," International Symposium on Electromachining-ISEM XV, 2007, pp. 381-386.

[6] M. J. Klopfstein, R. Ghisleni, D. A. Lucca, and E. Brinksmeier, "Surface Characteristics of Micro-Ultrasonically Machined (1 0 0) Silicon," International Journal of Machine Tools and Manufacture, 2008, vol. 48, no. 3, pp. 473-476.

[7] M. M. Sundaram, S. Cherku, and K. P. Rajurkar, "Micro Ultrasonic Machining Using Oil Based Abrasive Slurry," Proceedings of the International Conference on Manufacturing Science and Engineering (MSEC), 2008, pp. 221-226.

[8] Z. Yu, X. Hu, and K. P. Rajurkar, "Study of Micro Ultrasonic Machining of Silicon," Proceedings of ASME International Mechanical Engineering Congress and Exposition, 2005, pp. 1-8.

[9] K. Egashira, and T. Masuzawa, "Microultrasonic Machining by the Application of Workpiece Vibration," Annals of the CIRP, 1999, vol. 48/1, pp. 131-134.

[10] B. H. Yan, A. C. Wang, C. Y. Huang, and F. Y. Huang, "Study of Precision Micro-holes in Borosilicate Glass using Micro EDM Combined with Micro Ultrasonic Vibration Machining," International Journal of Machine Tools and Manufacture, 2002, vol. 42, no. 10, pp. 1105-1112.

[11] Z. Y. Yu, K. P. Rajurkar, and A. Tandon, "Study of 3D Micro-Ultrasonic Machining," Journal of Manufacturing Science and Engineering, 2004, vol. 126, no. 4, pp.727-732.

[12] Y. Yang, and X. Li, "Micro Ultrasonic Machining of Ceramic MEMS with Micro Metallic Dies," Proceeding of ASME International Mechanical Engineering Congress, 2003, pp. 93-95.

[13] K. Egashira, T. Taniguchi, H. Tsuchiya, and M. Miyazaki, "Microultrasonic Machining Using Multitools," Proceedings of the Seventh International Conference on Progress Machining Technology, 2004, pp. 297-301.

[14] C. Zhang, E. Brinksmeier, and R. Rentsch, "Micro-USAL Technique for the Manufacture of High Quality Microstructures in Brittle Materials," Precision Engineering, 2006, vol. 30, no. 4, pp. 362-372.

[15] K. Egashira, T. Masuzawa, M. Fujino, and X. Q. Sun, "Application of USM to Micromachining by On-the-Machine Tool Fabrication," International Journal of Electrical Machining, 1997, no. 2, pp. 31-36.

[16] X. Q. Sun, T. Masuzawa, and M. Fujino, "Micro Ultrasonic Machining and Self-Aligned Multilayer Machining/Assembly Technologies for 3D Micromachines," Proceedings of the Annual International Workshop on Micro Electro Mechanical Systems, 1996, pp. 312-317.

[17] T. Tateishi, N. Yoshihara, J. Yan, and T. Kuriyagawa, "Fabrication of High-Aspect Ratio Micro Holes on Hard Brittle Materials -Study on Electrorheological Fluid-Assisted Micro Ultrasonic Machining," Key Engineering Materials, 2009, vol. 389, pp. 264-270.

[18] D. Hoover, and D. Kremer, "Milli Newton Force Measurement and Control for Micro Ultrasonic Machining," International Symposium on Electromachining-ISEM XV, 2007, pp. 375-379.

[19] A. Curodeau, J. Guay, D. Rodrigue, L. Brault, D. Gagné, and L. P. Beaudoin, "Ultrasonic Abrasive μ-Machining with Thermoplastic Tooling," International Journal of Machine Tools and Manufacture, 2008, vol. 48, no. 14, pp. 1553-1561.

[20] X. Hu, Z. Yu, and K. P. Rajurkar, "Experimental Study of Tool Wear in Micro Ultrasonic Machining," Transactions of NAMRI/SME, 2007, vol. 35, pp. 129-136.

[21] T. Kuriyagawa, T. Shirosawa, O. Saitoh, and K. Syoji, "Development of Micro Ultrasonic Abrasive Machining System (1st Report, Studies in Micro Ultrasonic Abrasive Machining)," JSME International Journal Series C, 2002, vol. 45, no. 2, pp. 593-600.

[22] B. Jia, W. Bian, W. Zhao, and Z. Wang, "Study to Enhance the Micro-level in USM," International Conference on Integration and Commercializations of Micro and Nano Systems, 2007, pp. 1541-1545.

[23] Z. Yu, X. Hu, and K. P. Rajurkar, "Influence of Debris Accumulation on Material Removal and Surface Roughness in Micro Ultrasonic Machining of Silicon," Annals of the CIRP, 2006, vol. 55/1, pp. 201-204.

[24] System Identification Toolkit User Manual, National Instruments, 2004.

[25] P. Andersen, "Identification of Civil Engineering Structures Using Vector ARMA Models," PhD Dissertation, Aalborg University, 1997.

[26] Z. Y. Wang, and K. P. Rajurkar, "Dynamic Analysis of the Ultrasonic Machining Process," Journal of Manufacturing Science and Engineering, 1996, vol. 118, no. 3, pp. 376-381.

[27] M. Wiercigroch, R. D. Neilson, and M. A. Player, "Material Removal Rate Prediction for Ultrasonic Drilling of Hard Materials using an Impact Oscillator Approach," Physics Letters A, 1999, vol. 259, no. 2, pp. 91-96.

[28] K. P. Rajurkar, and W. M. Wang, "Real-Time Stochastic Model and Control of EDM," Annals of CIRP annals, 1990, vol. 39/1, pp. 187-190.

[29] M. A. Elbestawi, K. M. Yuen, A. K. Srivastava, and H. Dai, "Adaptive Force Control for Robotic Disk Grinding," Annals of CIRP, 1991, vol. 40/1, pp. 391-394.

[30] L. Rubio, and M. de la Sen, “Adaptive Control of Milling Forces under Fractional Order Holds,” Innovative Algorithms and Techniques in Automation, Industrial Electronics and Telecommunications, 2007, pp. 257–261.

[31] E. Brinksmeier, and C. Popp, “A Selftuning Adaptive Control System for Grinding Processes,” Annals of the CIRP, 1991, vol. 40/1, pp. 355–358.

[32] W. C. Pitstra, and J. K. Pieper, “Controller Designs for Constant Cutting Force Turning Machine Control,” ISA Transactions, 2000, vol. 39, no. 2, pp. 191-203.

[33] C. Xu , and Y. C. Shin, “Control of Cutting Force for Creep-Feed Grinding Processes Using a Multi-Level Fuzzy Controller,” Journal of Dynamic Systems, Measurement, and Control, 2007, vol. 129, no. 4, pp. 480-492.

[34] H. E. Jenkins, and T. R. Kurfess, “Adaptive Pole-Zero Cancellation in Grinding Force Control,” IEEE Transactions on Control Systems Technology, 1999, vol. 7, no. 3, pp. 363-370.

[35] M. S. Cheong, D. Cho, and K. F. Ehmann, “Identification and Control for Micro-Drilling Productivity Enhancement,” International Journal of Machine Tools and Manufacture, vol. 39, no. 10, 1999, pp. 1539-1561.

[36] LabVIEW PID Control Toolkit User Manual, National Instruments, 2006.

[37] L. Rubio, M. de la Sen, and A. Ibeas, “Discrete-Time Model Reference Control of Milling Forces under Fractional Order Hold Part II: Extensions to Adaptive Control,” IEEE Conference on Emerging Technologies and Factory Automation, 2006, pp.1005-1008.

[38] W. M. Wang, and K. P. Rajurkar, “Modeling and Adaptive-Control of EDM Systems,” Journal of Manufacturing Systems, 1992, vol. 11, no. 5, pp. 334-345.

[39] K. J. Åström, and B. Wittenmark, “Adaptive Control,” Addison Wesley, 1995.

APPENDIX A

The figure below shows the Simulink computer simulation model structure for the cutting force prediction based on the ARMAX model.

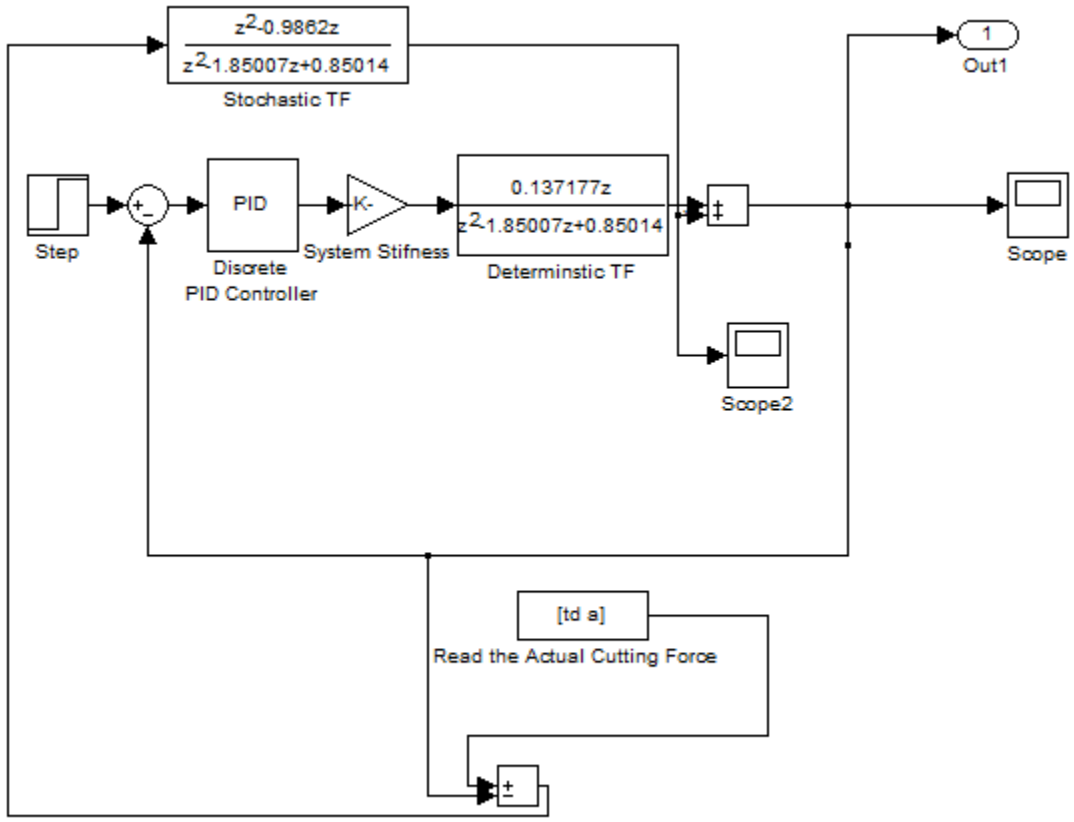

APPENDIX B

The figure below shows the Simulink computer simulation model for the cutting force under the PID controller (the P and the PI controllers are special cases) based on the ARMAX model.

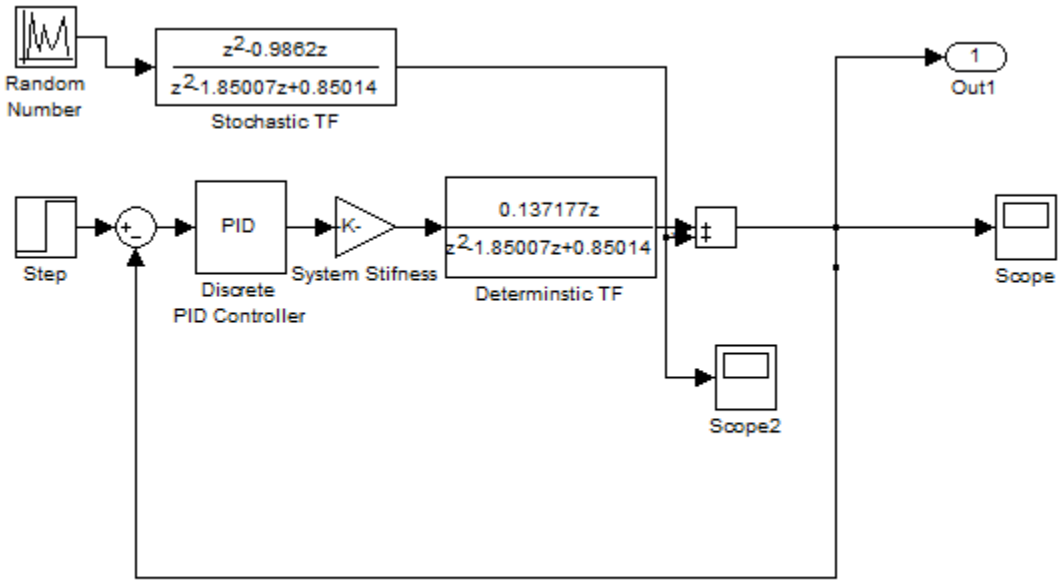

APPENDIX C

The figure below shows the Simulink computer simulation model for the cutting force control under the MRAC controller based on the ARMAX model.